Preprints (www.preprints.org) | NOT PEER-REVIEWED | Posted: 27 July 2022 doi:10.20944/preprints202203.0290.v2

New Workflow Predicts Drug Targets against SARS-CoV-2 via Metabolic Changes in Infected Cells

Nantia Leonidou[1,2,3,*], **Alina Renz**[1,2,3], **Reihaneh Mostolizadeh**[1,2,4], and **Andreas Dräger**[1,2,3,4]

[1]Computational Systems Biology of Infections and Antimicrobial-Resistant Pathogens, Institute for Bioinformatics and Medical Informatics (IBMI), University of Tübingen, 72076 Tübingen, Germany
[2]Department of Computer Science, University of Tübingen, 72076 Tübingen, Germany
[3]Cluster of Excellence 'Controlling Microbes to Fight Infections', University of Tübingen, Germany
[4]German Center for Infection Research (DZIF), partner site Tübingen, Germany
[*]Correspondence: nantia.leonidou@uni-tuebingen.de

ABSTRACT

COVID-19 is one of the deadliest respiratory diseases, and its emergence caught the pharmaceutical industry off guard. This study presents a novel workflow to predict robust druggable targets against emerging RNA viruses using metabolic networks and information of the viral structure and its genome sequence. For this purpose, we implemented pymCADRE and PREDICATE to create tissue-specific metabolic models, construct viral biomass functions and predict host-based antiviral targets from one or more genome sequences. We observed that pymCADRE reduces the computational time of flux variability analysis for internal optimizations. We applied these tools to create a new metabolic network of bronchial epithelial cells infected with SARS-CoV-2 and identified enzymatic reactions with inhibitory effects. The most promising reported target was the Nucleoside Diphosphate Kinase (NDPK1), for which the literature reports inhibitors. Additionally, we predicted further lipids-related enzymatic candidate targets that involve cholesterol, phospholipids and sphingolipids. Finally, we computationally tested the robustness of our targets in all known variants of concern, verifying NDPK1's inhibitory effect. Since our workflow focuses on metabolic fluxes within infected cells, it is applicable for rapid hypothesis-driven identification of potentially exploitable antivirals concerning various viruses and host cell types.

Availability: https://github.com/draeger-lab/pymCADRE/.

Keywords: pymCADRE; host-virus interactions; tissue-specific model; COVID-19; SARS-CoV-2; antiviral targets; flux balance analysis; flux variability analysis; reaction knockout; host-derived enforcement; metabolic modeling; virus mutations; nucleoside diphosphate kinase; software engineering; Python

Introduction

In a study published in October, 2007, scientists studying coronaviruses characterized the situation in China as a ticking "time bomb" for a potential virus outbreak[1]. They had three strong indications to worry: the animal-related eating habits in southern China, the previous appearance of Severe Acute Respiratory Syndrome Coronavirus (SARS-CoV)-like viruses in horseshoe bats, and the ability of coronaviruses to undergo recombination. Since the first major pandemic of the new millennium in 2002, over 4,000 publications on coronaviruses became available, giving insights and leading to the discovery of 36 SARS-related coronaviruses in humans and animals. Eighteen years later, the whole world experiences the realization of this prophecy with the emergence of the Coronavirus Disease 2019 (COVID-19) to be one of the deadliest respiratory disease pandemics since the "Spanish" influenza in 1918[2]. Scientists globally try to understand the host's immunopathological response, how the novel virus Severe Acute Respiratory Syndrome Coronavirus 2 (SARS-CoV-2) adapts, and how it spreads.

Viruses, being infectious agents, replicate only within the cells of a living organism and re-program them to form other virus particles and accelerate their own reproduction. Their life cycle is divided into four main steps: host cell attachment, penetration, reproduction within the host cell (uncoating, gene expression, replication, and assembly), and release[3]. To increase their mass production, they consume energy from the host cell. This dependency is proved by experimental findings showing considerable metabolic flux alterations in host cells upon infection[4]. To this end, engineering the host metabolism to govern viral infections is of great interest. In fact, one of the largest classes of small-molecule antiviral drugs, the nucleoside and nucleotide analogs, target metabolic enzymes in the nucleotide synthesis resulting in a nucleotide pool imbalance[5]. Examples of such analogs that are already used against RNA viruses are ribavirin[6], acyclovir[7], and remdesivir[8]. Systems-level analysis of gene knock-outs upon bacterial infection with bacteriophage lambda also revealed metabolic genes that, when knocked-out, prevented the phage from replication[9], confirming the engineering of host metabolism as a virus growth regulator.

These laboratory findings highlight the impact of viral

Preprints (www.preprints.org) | NOT PEER-REVIEWED | Posted: 27 July 2022 doi:10.20944/preprints202203.0290.v2

biosynthesis on host metabolism and the importance of metabolic alterations in the virus growth minimization. Hence, finding a suitable Virus Biomass Objective Function (VBOF) that reflects the functions of the infected cell is of immense interest. The VBOF is a pseudo-reaction simulating the production of the different virus particles and is analogous to the biomass function used for the metabolic models of prokaryotes and eukaryotes. It consists of energy metabolites, nucleotides, and amino acids, essential for the replication and production of genetic material and proteins. In 2018, Aller *et al*. presented a computational approach to create viral objective functions and predicted critical host reactions of the human macrophages against epidemic viruses, like the Zika virus[10]. The applicability of their method was verified by recovering antecedent antiviral targets and predicting new ones.

Notwithstanding the recent therapeutic advances and the approval of multiple vaccines, COVID-19 remains a substantial global health threat. Currently, great efforts are initiated to detect effective antiviral treatments for this pathogenic agent. Like all viruses, SARS-CoV-2 continuously evolves over time as modifications in its genome occur during replication. Such alterations are typical for viruses that encode their genome in RNA, as enzymes that copy the ribonucleic acid are prone to making errors leading to the presence of copying mistakes during viral replication[11]. It has been reported that SARS-CoV-2, along with all coronaviruses, has relatively low mutation rates ($\sim 1 \cdot 10^{-6}$ per site per cycle) compared to other RNA viruses, like HIV-1 or influenza viruses[12,13]. This is ascribed to the presence of proofreading and error-correcting enzymes that recognize and repair copying mistakes hindering the development of anti-CoV drugs and vaccines[14]. SARS-CoV-2 encodes an exonuclease (ExoN) in the non-structural protein 14 (NSP14), which participates in the genome proofreading mechanism and results in low mutation rates (or high viral fidelity)[15,16]. The 5' region of the SARS-CoV-2 genome encodes for two open reading frames (ORF1a/ORF1ab and ORF1b) which include 16 non-structural proteins (NSPs)[17,18]. These are followed by four structural proteins: nucleocapsid (N), envelope (E), the spike (S) and the membrane (M), and nine accessory proteins (NS)[17,18].

At the time of writing, five variants of SARS-CoV-2 have been designated as Variants of concern (VOC) by the World Health Organization (WHO). These are the Alpha (14$^{\text{th}}$ December, 2020, United Kingdom (UK), lineage B.1.1.7), Beta (18$^{\text{th}}$ December, 2020, South Africa, lineage B.1.351), Gamma (2$^{\text{nd}}$ January, 2021, Brazil, lineage P.1), Delta (24$^{\text{th}}$ March, 2021, India, lineage B.1.617), and Omicron (24$^{\text{th}}$ November, 2021, South Africa/Botswana, lineage B.1.1.529) variants[19]. These differ from the conventional virus in terms of their pathogen properties (e.g., transferability, virulence, or susceptibility to the immune response of recovered or vaccinated people). Mutations on the structural proteins occur most frequently and issue complications en route to pathogenesis. The most common mutation of the S protein is the non-synonymous replacement of aspartate by glycine (D614G), which is found to decrease the virus effectivity[20]. Mutations in the E protein have not been reported in any variants, except the Beta and Omicron. These are the substitution of proline by leucine (`P71L`)[21], and the exchange of the hydrophilic threonine by the hydrophobic isoleucine (`T9I`)[22].

Identifying potential targets and druggable compounds is of vast concern, and one way to detect them is by analyzing metabolic changes in infected cells. This can be achieved with the help of systems biology and the reconstruction of cell-specific Genome-scale Metabolic Models (GEMs) that recapitulate the metabolism of particular cell types[23,24]. Targeting the host metabolism has already been suggested as a prospective novel antiviral approach, given the relevance of metabolism in virus infection[25]. Since the emergence of SARS-CoV-2 and within a year several studies have been published trying to identify antiviral targets using constraint-based metabolic modeling and utilizing various approaches and resources[26–31]. For instance, a recent study by Bannerman *et al*. used a draft model of the airway epithelial cells built from Recon1[32], refined it using Recon3D[33] further databases, and predicted drug targets against SARS-CoV-2. However, they used pre-existing reconstruction tools and models to obtain a representation of the tissue metabolism.

In 2012 Wang *et al*. published the metabolic Context-specificity Assessed by Deterministic Reaction Evaluation (mCADRE) algorithm to construct metabolic models based on human gene expression data and network topology information. This tool is implemented in MATLAB[34], and its functionality is based on the first version of the human model, namely Recon1[32]. This resulted in its limited usability in the last few years since MATLAB is a commercial and closed-source software.

Here, we present pymCADRE, a re-implementation of mCADRE in Python striving for a more accessible and updated version of the reconstruction tool. Additionally, we implemented scripts for data pre-processing facilitating relevant curation tasks, such as assigning confidence scores to reactions, binarizing raw transcriptomic data, and calculating gene ubiquity scores. Pathological studies already pointed out that SARS-CoV-2 targets the airways and the lungs[35,36]. The entry and infectivity of enveloped viruses are strongly regulated by proteolytic cleavage of the viral envelope glycoproteins[37]. In the case of SARS-CoV-2, the S protein, when bound in the cell surface, is susceptible to airway protease cleavage, which results in conformational change favoring the entry of the virus[37] into human bronchial epithelial cells. Further single-cell analyses provided insights into the virus replication and the cell tropism, confirming that infection with SARS-CoV-2 is also localized in the bronchial epithelial cells[38,39]. Hence, we applied pymCADRE to create a novel tissue-specific model of the human bronchial epithelial cell (BEC1) based on the already available human metabolic network, Recon1. We updated the model by including a biomass maintenance function Bordbar *et al*. published in

Preprints (www.preprints.org) | NOT PEER-REVIEWED | Posted: 27 July 2022 doi:10.20944/preprints202203.0290.v2

2010[40].

We subsequently infected this model *in silico* with the novel SARS-CoV-2 virus by constructing a viral biomass reaction derived from its structural information. Therefore, we created a fully automated computational tool in Python, Prediction of Antiviral Targets (PREDICATE), which applies the stoichiometric approaches introduced by Aller *et al*. on a metabolic network, constructs a single VBOF, and creates an integrated host-virus model[10]. These approaches have already been extended and employed in the context of SARS-CoV-2[27,30] also regarding a distinct tissue type, the human macrophages[26]. Subsequently, our tool predicts exploitable cellular metabolic pathways that can be inhibited to suppress virus replication with minimal or no effect on the cell. This is attained using two approaches: the Host-derived enforcement (HDE)[10] and single-reaction knock-outs. We applied our automated script to our tissue-specific model Recon1-BEC1 and detected potential host-based targets for future COVID-19 therapeutic strategies. We further used our tool and validated the robustness of our predicted targets against all five variants of concern. We underline the identified metabolic reactions as experimentally exploitable drug targets for suppressing SARS-CoV-2 replication in human bronchial epithelial cells. We syntactically validated our model and compared it against the corresponding model reconstructed using mCADRE.

Altogether, our novel workflow can be summarized in a four-step process, as shown in Figure 1, which is fully transferable to any existing RNA virus and any host cell. With this we aim to further support the development of effective therapies against emerging viruses and their mutations.

Results

Tissue-specific reconstruction using pymCADRE

The pymCADRE tool was developed to reconstruct tissue-specific metabolic models based on human gene expression data and topological information from the metabolic network. Like mCADRE, pymCADRE leverages gene expression microarray data, literature-derived evidence, and information from the network topology to build context-specific metabolic models. More accurately, it uses a fully automated way to determine core reactions by setting a threshold to expression-based evidence. Therefore, reactions with scores above this threshold are characterized as core reactions, while the rest constitute the non-core set (more details in the Material and Methods section). To test the functionality of pymCADRE and increase its ability to create multiple models of human cells, specifically related to the current outbreak of SARS-CoV-2, we applied pymCADRE to a microarray expression profile dataset of the human bronchial epithelial cell (BEC1). Prior to reconstruction, we incorporated a Biomass Objective Function (BOF) to the first version of the human metabolic network, Recon1[32], and used it as a generic host human model.

The objective function originates from the human alveolar macrophage model published by Bordbar *et al*. in 2010 (supplementary file S0)[40]. We updated the resulting model by adding subsystems to all the missing metabolic reactions from Recon1. A subsystem-wise classification in Figure 2 indicates that most reactions in the final Recon1-BEC1 model belong to the class of transport reactions, while the biosynthesis of other secondary metabolites is the least represented subsystem. Moreover, in Recon1, there is no growth medium defined, and all extracellular transport reactions are open, i.e., lower fluxes equal $-1{,}000.0\,\mathrm{mmol}/(\mathrm{gDW}\cdot\mathrm{h})$. Additionally, we defined a minimal growth medium using the Constraints-Based Reconstruction and Analysis for Python (COBRApy)[43] package with necessary components. The exact minimal medium definition is provided in the supplementary file S3.

The new integrated tissue-specific model Recon1-BEC1 contains 1,341 reactions, 1,081 metabolites, and 1,044 genes (Table 1). Almost 70 % of all reactions is associated to a gene-protein-reaction rule (930; 775 metabolic and 155 transport reactions), while 248 metabolic and 164 transport reactions are not related to any gene. We observed that pymCADRE reduces the pruning time while maintaining the highest possible accuracy compared to the model created with mCADRE (Table 1). With a 3.3 GHz processor and 16 GB random-access memory (RAM) on a local computer, mCADRE with FVA demanded ∼6 CPU-hours, while pymCADRE ∼5 CPU-hours. Totally 1,272 blocked reactions were eliminated from Recon1 during the consistency check. Furthermore, 1,130 reactions (36 core and 1,094 non-core) were inactive in the cell type of interest and removed from the generic model during pruning. Inconsistencies were encountered in the performance of FASTCC as implemented in COBRApy. After multiple runs, the function detected a variable number of blocked reactions. This affected the final pruned model, which differed from the ground truth. However, internal optimizations with FASTCC were executed faster compared to FVA. Duplicating the available RAM can reduce the computational time of the pymCADRE twofold.

After the tissue-specific reconstruction, we refined the model using Recon3D[33] and HumanCyc[45]. We further extended the models by adding missing exchange reactions to all extracellular metabolites (42 in the mCADRE and 43 in the pymCADRE model). The final reconstructions shared over 1,370 reactions, meaning an overlap of 99 % of all reactions in each model. Hence, we have a considerable convergence between the tools, indicating the high quality of models generated with pymCADRE. Table 2 lists the symmetric difference between both models.

Additional analysis using Flux Balance Analysis (FBA) allowed us to study the flux dispersion between the host and virus and conclude which reactions are vital for both host maintenance and virus growth. Explanatory Data Analysis (EDA) showed that non-zero fluxes are mostly fluctuating above zero (Figure 3a). Totally 19 numerically distant values (outliers) were observed (Figure 3b). Inspection of the flux distribution vector showed that there is higher flux through the carbon metabolism (ENO, GAPD, LDH_L, PGK, PGM, PYK,

Preprints (www.preprints.org) | NOT PEER-REVIEWED | Posted: 27 July 2022 doi:10.20944/preprints202203.0290.v2

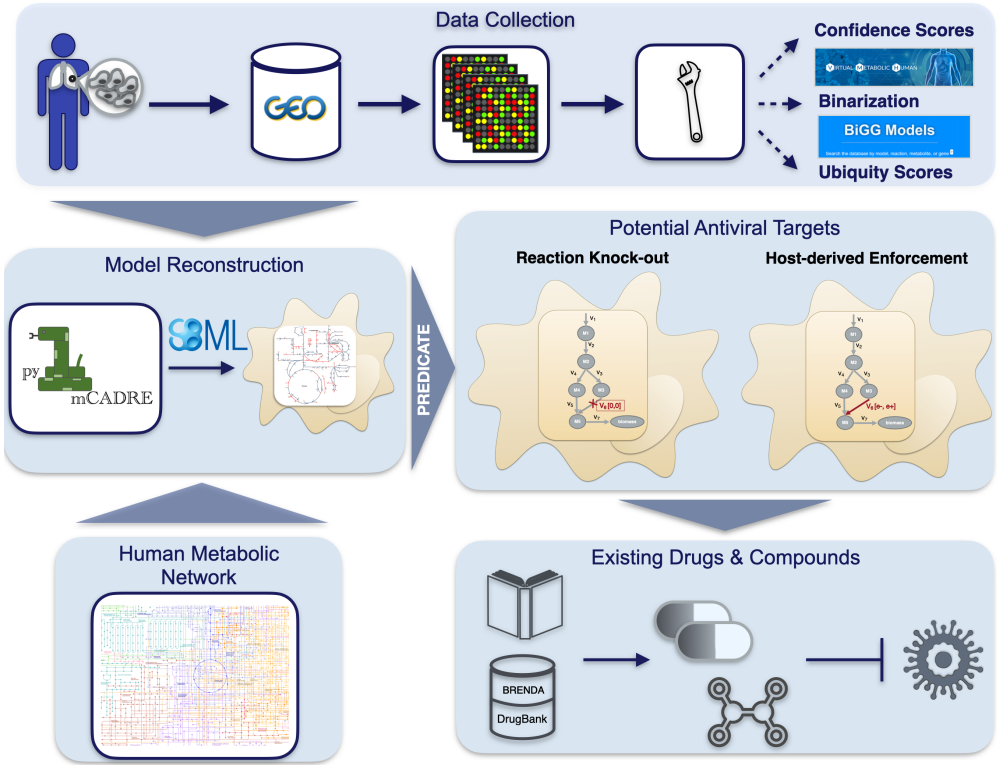

Figure 1. Workflow overview to reconstruct integrated host-virus genome-scale models and detect promising compounds with an antiviral activity. After collecting and curating the required data (the gene expression data and the human metabolic network), pymCADRE reconstructs a tissue-specific model using information from the network topology. The reconstructed metabolic network is then infected *in silico* with the virus of interest and is used to detect promising antiviral targets in an automated process. Detailed description of the process and the respective algorithm, called PREDICATE, is provided in Figure 7. Reaction knock-outs and the host-derived enforcement are used to detect exploitable enzymatic targets that keep the host maintenance at 100 %, while suppressing the virus replication. The resulted top hits are further inspected manually in terms of already existing drugs and compounds in different databases, such as BRENDA[41] and DrugBank[42].

TPI, and FBA). Furthermore, the glutamate dehydrogenases (GDHm and GLUDym) are used remarkably more by the virus to achieve the optimal growth state, compared to the host cell.

Similar to mCADRE, pymCADRE encompasses functionality tests to ensure the fulfillment of the resulting models' basic cellular metabolic capabilities. These tests include the production of various metabolites, such as amino acids and compounds from the Tricarboxylic Acid Cycle (TCA) when the uptake of glucose is enabled[46]. Additional to this, we tested our model for internal cycles that result in erroneous energy production by testing the production of different energy metabolites when no nutrients are available.[47] Our final model did not include any futile cycles since none of the metabolites could be generated.

The new tissue-specific model created with pymCADRE was converted into SBML Level 3 Version 2[48] format using the Systems Biology Format Converter (SBFC)[49] and passed the syntactical validation using libSBML[50]. Additionally, the Metabolic Model Testing (MEMOTE) suite Version 0.11.1 was used to assess the GEM quality[51]. MEMOTE reports for a given GEM an independent and comparable score along with a comprehensive overview. This test reported a score of 70 % for our integrated model, which indicates a well-annotated model. Other similar models posses lower quality scores[30,40,46] compared to our Recon1-BEC1 model.

To test that pymCADRE functions as expected, we implemented test scripts, which are available at https://github.com/draeger-lab/pymCADRE/.

Since we purposed to use the model to detect possible anti-SARS-CoV-2 targets, we also included a VBOF that imitates the production of virus particles from its different constituents. Following the pipeline developed by Aller *et al.*[10] and extended by Renz *et al.*[52], we created this pseudo-reaction and used it to infect the new model (Recon1-BEC1) *in silico*. The human bronchial epithelial cell's biomass maintenance function (BOF) encompasses amino acids, DNA and RNA nucleotides, and compounds vital for energy supply, and other macromolecules like fatty acids and phospholipids. Similarly, the VBOF contains amino acids, RNA, lipids, and energy-related compounds (Table A4, Figure A13), as well necessary lipids. Analysis of both functions highlights leucine as the most-used amino acid (highest stoichiometric coeffi-

Preprints (www.preprints.org) | NOT PEER-REVIEWED | Posted: 27 July 2022 doi:10.20944/preprints202203.0290.v2

Table 1. Analysis results of the BEC1-specific reconstructions using Flux Variability Analysis (FVA) for internal optimizations. The reaction overlap between both models is at 99 %.

	Pruned Model			Removed Reactions	
	Reactions	Metabolites	Genes	Cores	Non-cores
mCADRE	1,343	1,080	1,905	36	1,092
pymCADRE	1,341	1,081	1,044	36	1,094

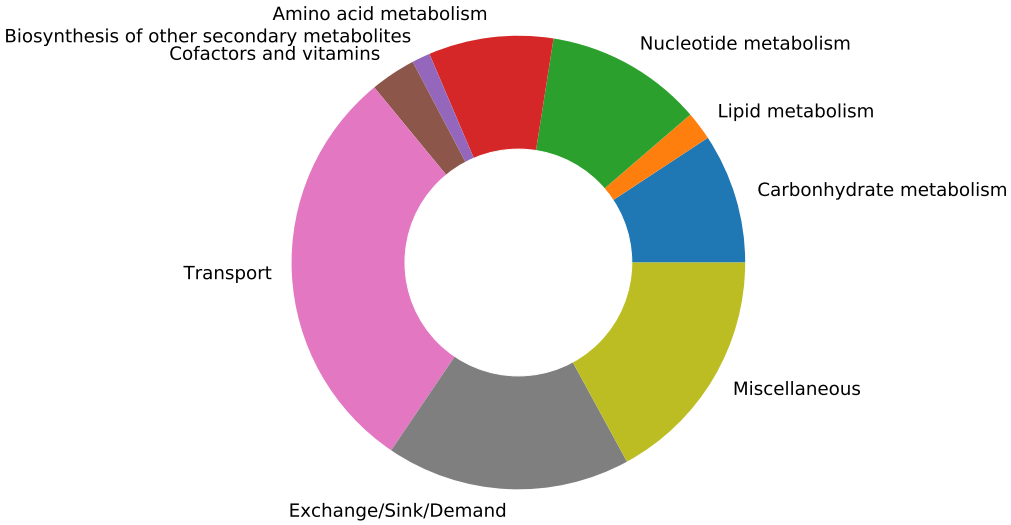

Figure 2. Subsystem-wise classification of all reactions included in Recon1-BEC1. The reaction pathways are merged based on metabolic pathways and according to Kyoto Encyclopedia of Genes and Genomes (KEGG)[44]. The biomass reaction was assigned to "Miscellaneous." The majority of reactions in the final Recon1-BEC1 model are transport reactions, while the least amount of reactions is assigned to the biosynthesis of other secondary metabolites subsystem.

cient) in the SARS-CoV-2 growth and the maintenance of the host bronchial cells, while both host and virus utilize only a few tryptophan (Figure 4). Moreover, the same amount of asparagine and phenylalanine is required for the maintenance of the host cell, while the virus needs less phenylalanine. Similar pattern was observed for tyrosine and histidine. Using FBA, optimization of the Recon1-BEC1 for the host resulted in a flux for the biomass maintenance function of $0.099\,\mathrm{mmol}/(\mathrm{gDW}\cdot\mathrm{h})$, while optimizing the SARS-CoV-2 growth function resulted in a flux of $0.0113\,\mathrm{mmol}/(\mathrm{gDW}\cdot\mathrm{h})$.

Stoichiometric modeling of the integrated host-virus model predicts targets against SARS-CoV-2

To analyze the host-virus interactions from a metabolic point of view, we created an integrated stoichiometric model of human bronchial epithelial cells infected with SARS-CoV-2. We then used our model to detect host-based reactions, which, when constrained, reduce the virus production the most. According to Aller *et al.*, this analysis can be computationally implemented through systematically setting individual lower and upper bounds to zero (i.e., reaction knock-outs)[10]. Applying this approach, we identified a single target enzyme, which if knocked-out, completely inhibits the virus while keeping the host maintenance at 100 % of its initial growth rate. This enzyme is called NDPK1 (EC-Number: 2.7.4.6) and enables the conversion of Adenosine Triphosphate (ATP) and Guanosine Diphosphate (GDP) to Adenosine Diphosphate (ADP) and Guanosine Triphosphate (GTP) (KEGG Reaction ID: `R00330`):

$$\mathrm{ATP} + \mathrm{GDP} \rightleftharpoons \mathrm{ADP} + \mathrm{GTP}.$$

To verify our findings, we applied the HDE[10,52]. We constrained all reaction fluxes to ranges obtained from FVA, allowing the attainment of host-optimal state and suppressing the virus production at most. This approach verified the enzymatic target NDPK1 and revealed further possible compounds that could inhibit the viral production. The adapted bounds for NDPK1 led to a decrease in the virus growth of almost 63 % of its original value with no effect on the host's maintenance (100 % of the maintenance rate). Further 60 enzymatic targets with inhibitory effects on the virus production were reported using the HDE approach. These concerned, for instance, the transport and extracellular exchange of L-histidine (BiGG IDs: `HISt4` and `EX_hist__L_e`), as well as reactions

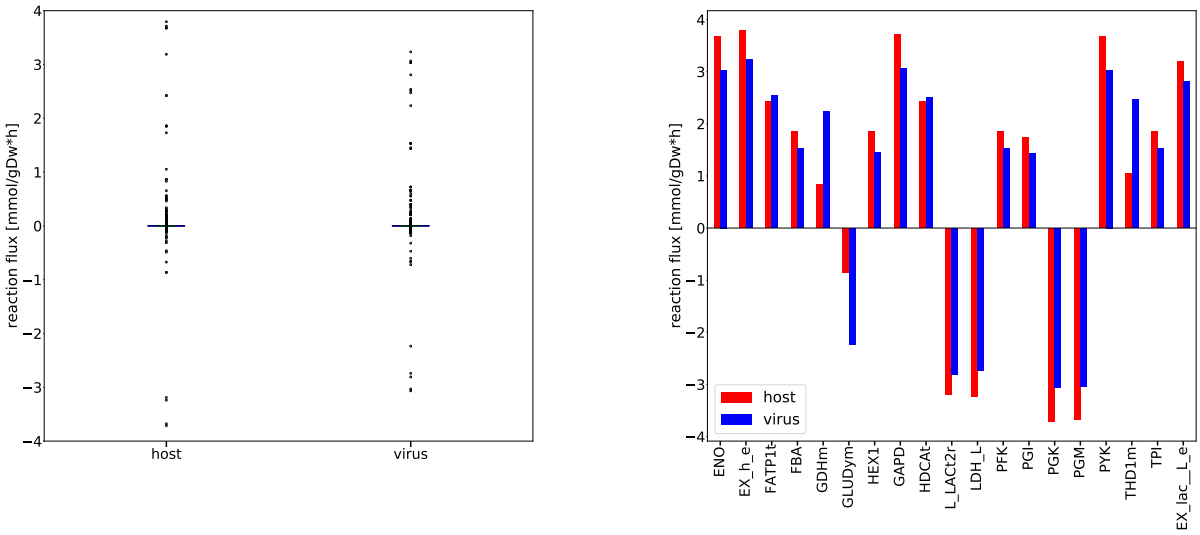

(a) The flux distributions were computed based on a five-number summary (Table A6). Remarkable outliers with a flux value greater than $1.0\,\mathrm{mmol}/(\mathrm{gDW}\cdot\mathrm{h})$ or less than $-1.0\,\mathrm{mmol}/(\mathrm{gDW}\cdot\mathrm{h})$ were investigated separately (b).

(b) The fluxes through `GDHm`, `GLUDym`, `HDCAt`, and `THD1m` are higher when the model is optimized for the virus growth. Overall, all displayed reactions are important for both the host maintenance and the virus growth.

Figure 3. Flux dispersion among host and virus in the Recon1-BEC1 model. Distribution of host and virus fluxes as derived from FBA.

Table 2. Symmetric difference of reactions in the models created by mCADRE and pymCADRE.

mCADRE	
`DM_dttp_m`	DTTP demand
`DNDPt20m`	DTDP transport via ATP antiport
`DTMPK`	DTMP kinase
`PROtm`	L-proline transport, mitochondrial
`ARTPLM2`	Palmitate conversion
`FUMtm`	Fumarate transport, mitochondrial
`G3PD1ir`	Glycerol-3-phosphate dehydrogenase (NAD+)
pymCADRE	
`DNDPt34m`	DGDP transport via dTDP antiport
`DNDPt44m`	DTTP transport via ATP antiport
`EX_glyc_e`	Exchange of glycerol
`GLYCt`	Glycerol transport via channel
`PROD2m`	Proline dehydrogenase, mitochondrial
`PIt2m`	Phosphate transporter, mitochondrial

from the cholesterol metabolism (`HMGCOARx`, `HMGCOAS`, `SQLEr`, and `LNSTLSr`), the terpenoid backbone biosynthesis (`DMATTx`, `IPDDIx`, `PMEVKx`, `DPMVDx`, `MEVK1x`, and `GRTTx`), and various transporters (e.g., `CO2ter`, and `PPItx`). These reactions, when constrained, could lead to a decrease in the viral production by 56 % to 58 % of the initial growth. Figure 5 illustrates all antiviral targets predicted using HDE against the percentage of the remaining virus growth after constraining the reaction bounds. Detailed information about all reactions is included in the supplementary material S1.

The Guanylate Kinase (GK1) (EC-Number: 2.7.4.8, KEGG Reaction ID: `R00332`) has been recently identified as an essential component for viral propagation and as a potential target for antiviral therapies against SARS-CoV-2 in the human alveolar macrophage model[26] and further cell lines[27,31]. Renz *et al*. firstly showed that `GK1` could decrease the virus production up to 50 % without damaging the macrophages' maintenance (100 %)[26]. Our host-derived enforcement on the bronchial epithelial cells also reported `GK1` as a potential anti-SARS-CoV-2 target, however, with lower impact on the virus production compared to `NDPK1`. Constraining `GK1` in our model resulted in 58.7 % virus production.

Interestingly, `NDPK1` is closely interconnected with the already identified robust target `GK1` in the purine metabolism (Figure 6). Both are transferases, and more specifically, phosphotransferases with a phosphate group as acceptor. `GK1` produces `GDP` which is subsequently used by `NDPK1` to generate `GTP`. Both `GDP` and `GTP` are catalyzed by the enzymes ribonucleoside-diphosphate (`RNDR2`) and ribonucleoside-triphosphate (`RNTR2`) reductase, respectively. Similarly, a decreased viral growth in the human bronchial epithelial cells could be caused by targeting neighboring enzyme, `NDPK1`. From this, we suggest that focusing on the purine metabolism, and more specifically on the action of one of the two enzymes to inhibit SARS-CoV-2 is a well-established approach that needs to be validated *in vitro* and in cell culture experiments.

Metabolic fluxes are highly affected by the nutrients' availability. Since our approaches mainly focus on studying the metabolic changes in infected cells, fluxes play a major role in the simulation outcomes. So far, we have focused on a

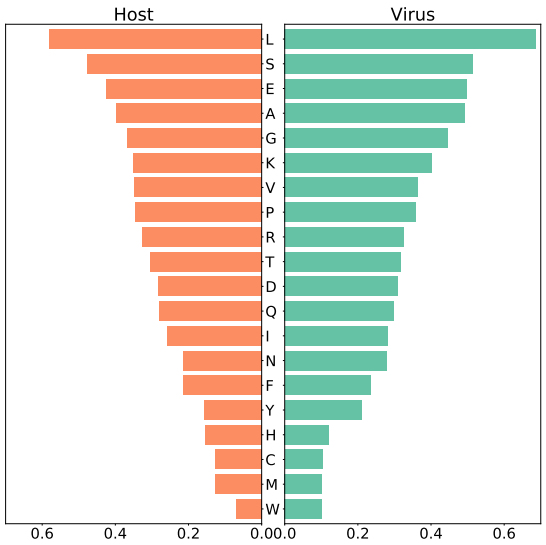

Figure 4. Amino acid usage between host and virus based on the stoichiometric coefficients. The two panels show the amino acid composition of the host maintenance function (left) and the virus biomass (right). The amino acids are annotated using the one-letter code (Table A5). Both host and virus use mostly leucine (L) for their maintenance/growth, while tryptophan (W) is needed at least. The same amount of asparagine (N) and phenylalanine (F) is required for the maintenance of the host cell, while the virus needs less phenylalanine. Similar pattern can be observed for tyrosine (Y) and histidine (H).

minimal growth medium computed using linear optimization[43]. Additionally, we examined the virus inhibition that our targets could reach using the blood medium[53]. With the blood medium defined, NDPK1 and GK1 showed the same inhibitory effect (single-reaction deletions: 100 % virus suppression, HDE: 62.5 % virus suppression) against SARS-CoV-2 and proved to be robust hits among various simulation conditions. Compared to the minimal defined medium, the inclusion of lipids in the composition of the viral biomass function using the blood medium resulted in a novel enzymatic hit target, the diacylglycerol acyltransferase (DGAT). DGAT resulted in a decrease of 66 % of the virus growth. This is a key enzyme in the lipid droplet formation and catalyzes the acyl-CoA-dependent synthesis of triacylglycerols from diacylglycerols. Although we observed a variation in the secondary resulted enzymatic targets when using different growth media, NDPK1 and GK1 remained robust and promising host-based targets. The HDE-derived metabolic targets using the blood medium are shown in Figure A10 and the medium definition is provided in the supplementary file S3.

Altogether, we created a fully automated computer tool, which simulates the virus growth in target cells with the help of metabolic networks. Subsequently, our tool applies the above-mentioned host-dependent approaches, host-derived enforcement, and reaction knock-outs, and predicts enzymatic targets with high inhibitory potency against the virus.

Predicted targets are robust against all known variants of concern

Novel mutations of RNA viruses emerge daily, and as of February, 2022, five SARS-CoV-2 variants have prevailed and spread since its emergence in 2019. These are the Alpha (B.1.1.7), Beta (B.1.351), Gamma (P.1), Delta (B.1.717.2), and Omicron (B.1.1.529) variants[19] and have been marked as VOC. Since the beginning of the COVID-19 pandemic, there has been an exponential growth in the number of stored genome sequences within large databases. The WHO asked all scientists around the world to upload their data on the Global Initiative on Sharing All Influenza Data (GISAID) database and help accelerate the response against health threats to humankind[56]. In January, 2020, the GISAID's EpiCoV™ database launched, becoming the most popular repository for SARS-CoV-2 as it gathers over eight million viral sequences by February, 2022. To examine the variants' effect on the predicted metabolic targets, sequences for all VOC were downloaded from GISAID and investigated further.

We reconstructed a SARS-CoV-2 VBOF using the same approaches as with the reference (wildtype) sequence for each retrieved mutated sequence. We reconstructed 100 individualized biomass functions and tested each to detect enzymes that inhibit the virus's growth while keeping the host maintenance at maximum. To speed up the reconstruction and analysis processes, we developed an automated script to analyze more than one sequence simultaneously (Figure 7). Additionally, we implemented an algorithm to modify reference protein sequences and introduce amino acid mutations (replacements, insertions, deletions, and duplications) and named this tool PREDICATE. Since RNA viruses are composed of similar building blocks, nucleotides, and proteins, our pipeline can be applied to any single- or double-stranded RNA virus that could infect any cell or tissue type.

To evaluate the mutations' effect on the viral biomass, we calculated the mean of all estimated coefficients across all mutated sequences and compared them against the Wild-type (WT) stoichiometries. We did this by looking at the variant-wise differences to the WT. Figure 8 shows how much the variant-wise calculated mean of coefficients deviates from the stoichiometries calculated for the reference sequence. We observed a remarkable increase in the stoichiometric coefficients of ATP and ADP between the Omicron variant and the WT. This pattern is mainly distinct to the ATP and ADP but is observed for the majority of the stoichiometric coefficients. We analyzed the mathematical calculations that led to the stoichiometric coefficients to explain this further. All coefficients depend on the total viral molar mass M_v, which is derived from the sum of the mass of the genome (G_i) and proteome (G_j)[10]. The randomly downloaded genomic sequences of the Omicron variant contained a higher amount of NNN stretches (i.e.,

Preprints (www.preprints.org) | NOT PEER-REVIEWED | Posted: 27 July 2022 doi:10.20944/preprints202203.0290.v2

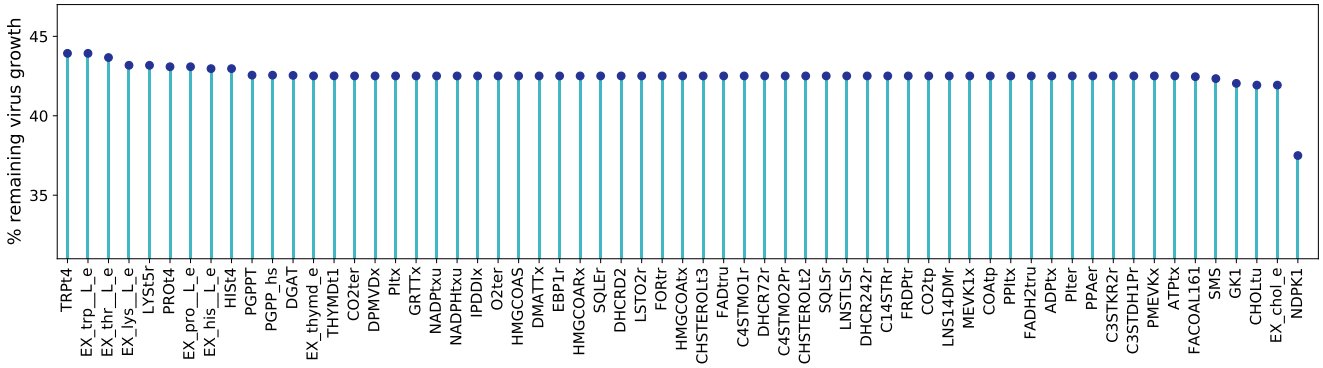

Figure 5. Enzymatic targets of SARS-CoV-2 from the HDE experiments applied to the Recon1-BEC1 model. Potential antiviral targets were reported when the virus rate of growth with shifted bounds was beneath the threshold of 50 % of its initial growth rate. NDPK1 with adapted bounds led to a remarkable virus decrease without affecting the host's maintenance.

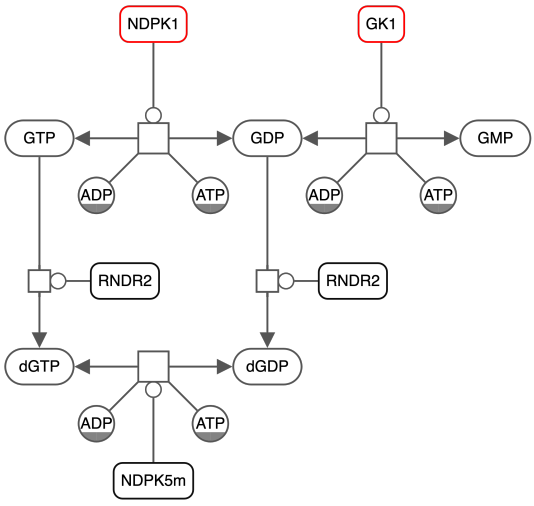

Figure 6. Graphical illustration of the interconnection between `NDPK1` and `GK1` in the purine metabolism using the Systems Biology Graphical Notation (SBGN)[54]. To annotate reactions and metabolites, Biochemcial, Genetical, and Genomical (BiGG) identifiers were utilized. Biological map created with Newt[55].

nucleotides that could not be determined via sequencing) compared to the other variants. Consequently, the Omicron variant has a decreased count of nucleotides (G_i) and amino acids (G_j), thus a lower total molar mass M_v. Moreover, the overall moles of energy (A^{TOT}) needed to assemble the structural and non-structural proteins strongly influences the stoichiometric coefficient of ATP[10]. The A^{TOT} is related to the total amino acids counts (X_j). Overall, the Alpha variant included more deletions in the spike (`H69del`, `Y144del`, and `V70del`) and NSP6 (`F108del`, `G107del`, and `S106del`) proteins compared to the Omicron variant. The same holds for the Beta, Gamma, and Delta variants. This affected the X_j, which was higher for the Omicron variant. Altogether, a decreased total viral molar mass and a higher total amino acids count resulted in the apparent rise of the ATP and ADP stoichiometric coefficients for the Omicron variant. Accordingly, the absolute differences between the WT and the Omicron variant are higher than the rest.

When looking at the differences between the amino acids and the WT stoichiometric coefficients, a noticeable increase in the Omicron Variant can be observed for lysine. For this reason, we inspected the respective amino acid mutations. In more than half of the Omicron-related genomic sequences, other amino acids were more often replaced by lysine (Spike `N440K`, Spike `N764K`, Spike `N856K`, Spike `N969K`, Spike `T478K`, Spike `N679K`, Spike `T547K`, and N `R203K`). In contrast, the substitution of lysine by other amino acids is rarely occurred (NSP3 `K38R` and Spike `K417N`). This also affected the stoichiometric coefficient of asparagine. As most of these mutations emerge in the spike protein, which has the highest copy number, their impact on the amino acid count, and consequently, the stoichiometric coefficient, is considerable. Among the variants for which a higher coefficient was computed for asparagine than the WT, the greatest increase was observed for the Delta variant. This could be justified by the presence of mutations, in which mostly an amino acid is being replaced by asparagine (Spike `D950N`, M `S197N`, NSP16 `H186N`, NSP3 `K1693N`, NSP8 `K37N`, and NSP3 `K902N`). A substitution of asparagine by another amino acid occurs only in three mutation types. Thus, overall there is an increase in the total amount of asparagine, and therefore, in the stoichiometric coefficient for the Delta variant. Lastly, the Omicron variant needs the least glutamine (−0.013) and the most lysine (0.015) compared to the WT.

To verify the validity of our calculations, we searched in the literature to find evidence about the amino acid composition of the different variants. For instance, we observed higher stoichiometric coefficients of charged and hydrophobic residues in the Omicron variant compared to the Delta. Recently, computational analyses indicated in the Omicron

Preprints (www.preprints.org) | NOT PEER-REVIEWED | Posted: 27 July 2022 doi:10.20944/preprints202203.0290.v2

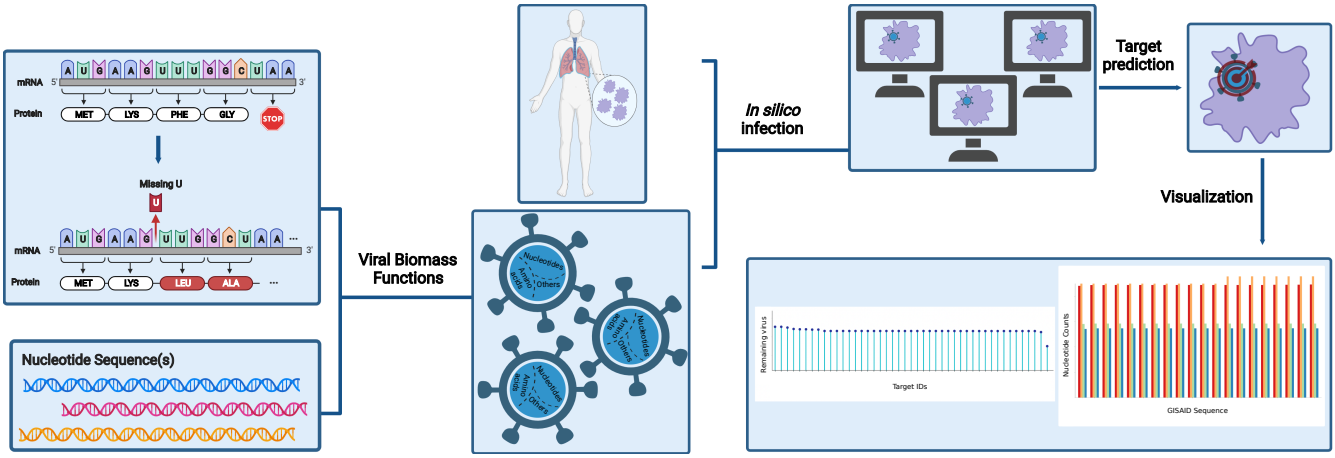

Figure 7. Overview of PREDICATE developed to create viral biomass reactions and predict host-based antiviral targets using host-virus models. First of all, our algorithm, PREDICATE, modifies the amino acids in the protein sequence according to the defined mutations. The mutated protein sequence and the nucleotide sequences are further employed to calculate the stoichiometric coefficients for the virus biomass functions. Reaction knock-outs and the host-derived enforcement are applied to reveal enzymatic reactions that suppress the viral replication. The final step generates various plots, providing insights into the dataset and a better understanding of the results. This pipeline can be applied to either one or more nucleotide sequences and all existing RNA viruses. This makes it particularly advantageous and time-saving when studying multiple variants of a single virus. The number of genomic input sequences equals the number of the calculated VBOF. The Materials and Methods section describes the implemented approaches to predict antiviral targets. Figure created with BioRender (BioRender.com).

variant an increased amount of arginine, lysine, aspartate, and glutamate that contribute to the formation of salt bridges[57]. The same study pointed out the accumulation of the hydrophobic residues, phenylalanine and isoleucine, in the spike protein of same variant[57].

After investigating the mutations' impact on the viral stoichiometric coefficients, we tested the effectiveness of the previously identified targets against the SARS-CoV-2 variants repeating the single-reaction deletions and HDE experiments. Our single-reaction knock-outs indicated NDPK1 to be the only potent antiviral inhibitor. All host-based targets detected from the HDE analysis to have an inhibitory effect on SARS-CoV-2 for all variants are shown in Figure 9. Targets were reported as potentially effective when the virus growth rate with altered bounds was lower than the threshold of 50 % of its initial growth rate. The NDPK1 was reported to have the highest virus inhibitory effect across all variants of concern. After its inhibition, the virus growth dropped to ∼37.5 % of its initial growth in the host cell. Further possible compounds were found to inhibit the viral production while keeping the host at maximum. Six enzymatic targets from the cholesterol metabolism and one transport reaction were detected to be WT-specific: DHCR242r, DHCR72r, LSTO2r, EBP1r, C3STDH1Pr, C4STMO2Pr, and LYSt4. Except for NDPK1, GK1 was a common target, which constraint led to a reduced virus growth (∼41.3 %), however not as effective as NDPK1. Moreover, the five SARS-CoV-2 variants shared eight additional hits with the WT that reported inhibitory effects. Our integrated host-virus model suggested the supplementation of L-histidine, L-threonine, L-lysine, L-proline, and L-tryptophan in the host's environment as potential targets with an inhibitory effect of ∼42 % to 43 % virus reduction, ensuring the cell's maintenance. Similarly, enforcing the import of L-proline, L-histidine, and L-tryptophan via the associated transport reactions (PROt4, HISt4, and TRPt4) reported same inhibitory effects and results in a virus suppression of ∼42 % to 43 % of the initial growth. Similar patterns of the inhibitory effect were observed between the five SARS-CoV-2 variants and the WT. Enriching the host's environment with L-choline, a phospholipid precursor, showed a remarkable inhibitory effect only for the WT and the Beta and Omicron variants.

Existing drugs and inhibitors could target predicted enzymes to hinder the growth of SARS-CoV-2

The computational approaches used here allowed the prediction of diverse enzymatic targets that could inhibit the SARS-CoV-2 replication in human bronchial epithelial cells. Single-reaction knock-out analysis reported a single possible antiviral target, namely NDPK1. The host-derived enforcement verified this target and predicted further 60 reactions. For these targets, we evaluated their corresponded enzymes considering already existing approved drugs using the BRENDA[41] and DrugBank[42] databases. We found various hitherto approved drugs and compounds that target some of the predicted reactions and could inhibit them, including those targeting the very promising enzymes NDPK1 and GK1. Table 3 lists examples of already existing drugs that inhibit

Preprints (www.preprints.org) | NOT PEER-REVIEWED | Posted: 27 July 2022 doi:10.20944/preprints202203.0290.v2

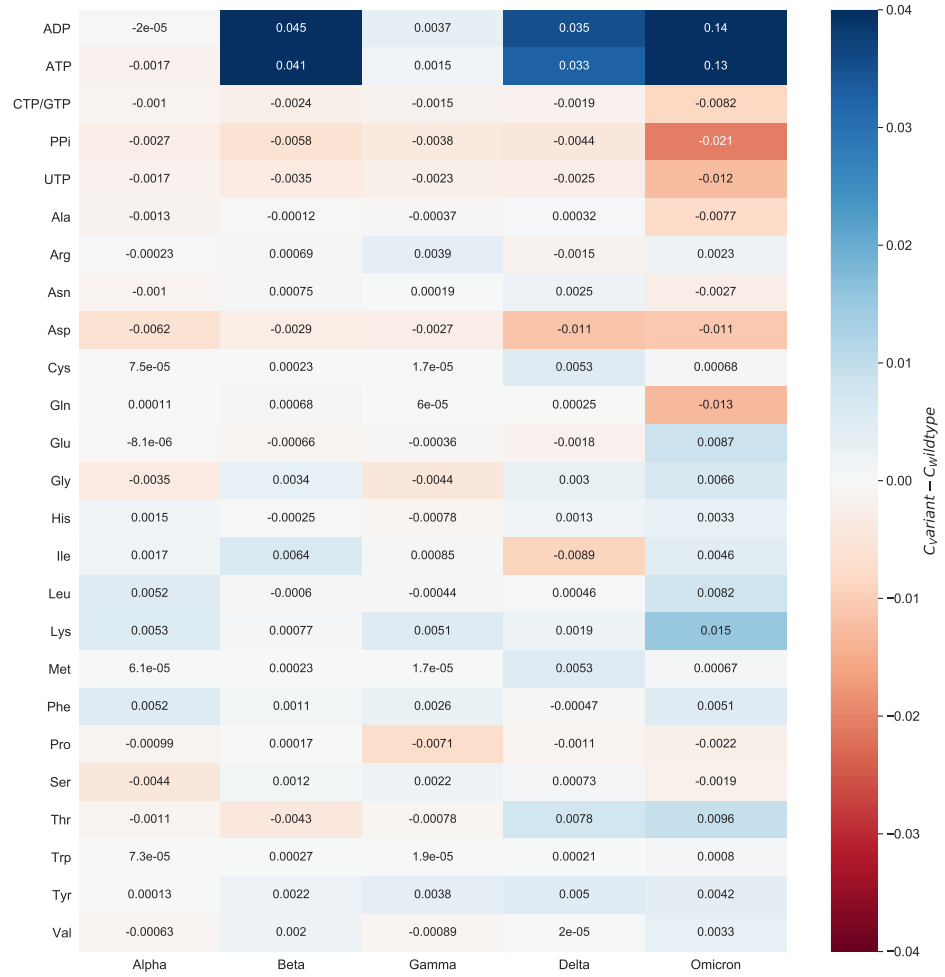

Figure 8. Variant-wise comparison of stoichiometric coefficients derived directly mutated sequences and the Wildtype. The difference between the average stoichiometric coefficients of the individual variants and the reference sequence was computed. Red color highlights decreased stoichiometric coefficients in the variants, while increased coefficients are colored by blue. A remarkable increase can be observed in the stoichiometric coefficients of ATP and ADP between the Omicron variant and the Wildtype. The stoichiometries of charged and hydrophobic amino acids were higher for the Omicron variant. All in all, the variations between mutants and Wildtype are very small.

our predicted anti-SARS-CoV-2 target reactions. These compounds and drugs could be used as an indication to validate the computational predictions made here experimentally.

Like all living cells, virus-infected cells require nucleotides to synthesize deoxyribonucleic and ribonucleic acid to strengthen their proliferation. Hence, nucleotide metabolism is regulated establish constant pools of pyrimidines and purines. Various drugs targeting the nucleotide metabolism in viral infections represent a therapeutic approach to limit viral replication. There are two main strategies to rewire the nucleotide metabolism: via purine and pyrimidine analogs (i.e., modified nucleosides used to stop DNA or RNA polymerase) or directly inhibiting the enzymes involved in DNA and RNA synthesis. Our predicted targets NDPK1 and GK1, are involved in the purine and pyrimidine metabolism.

We conducted extensive literature research and highlighted a nucleoside analog named acyclovir as an already approved drug against the action of `NDPK1` and `GK1` (Table 3). In acyclovir, the sugar in the deoxyguanosine is substituted by an acyclic side chain, a (2-hydroxyethoxy)methyl substituent, at position nine. The viral DNA polymerase is competitively inhibited by acyclovir which acts as an analog to deoxyguanosine triphosphate (dGTP). This results in chain termination since the adherence of further nucleosides is prevented by the absence of the 3'-hydroxyl group[62,63].

The second approach is the direct inhibition of enzymes related to nucleotide synthesis. In the past few years, diverse enzyme inhibitors have been known to treat viral infections. One such antiviral, merimepodib, targets the action of inosine-5'-monophosphate dehydrogenase (`IMPDH`) and has already beeen tested against emerging RNA viruses (e.g., Zika, Ebola, Lassa, Junin, and Chikungunya viruses)[64]. Dihydroorotate

Preprints (www.preprints.org) | NOT PEER-REVIEWED | Posted: 27 July 2022 doi:10.20944/preprints202203.0290.v2

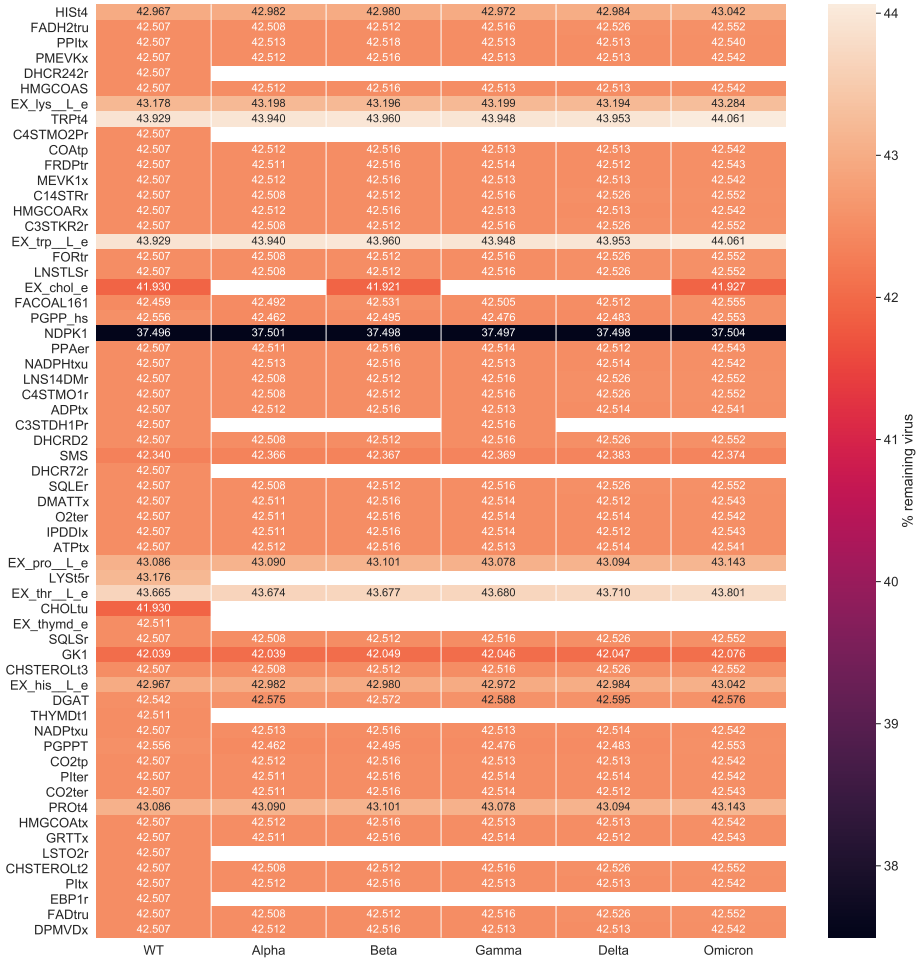

Figure 9. Results of the host-derived enforcement applied to all known variants of concern. The range and effect of reaction inhibitions on the VBOF were calculated while keeping the host's maintenance at 100 %. Only targets predicted across all retrieved sequences for a single variant were considered robust and were examined further. Empty cells in the heatmap represent targets that were not predicted as potential inhibitors for the corresponding variant. NDPK1 showed the highest inhibitory effect against the virus at all studied variants, followed by GK1. Enriching the host's environment with L-choline showed a remarkable inhibitory effect only for the WT and the Beta and Omicron variants.

dehydrogenase (DHODH) inhibitors have also been reported to be effective against arenaviruses in human cell lines[65]. However, knock-out analysis in these reactions reported a virus growth of 100 % in our bronchial epithelial cells model.

Additional examples of inhibitors that we identified with our methods are the 3-hydroxy-3-methylglutaryl-CoA (HMG-CoA) reductase (HMGCOARx) and the geranyltranstransferase (GRTTx). Both were reported as potential SARS-CoV-2 inhibitors showing 58.4 % virus reduction. The DrugBank and BRENDA databases list lovastatin and ibandronate as known drugs with known inhibitory effect against the two enzymesTable 3.

Conclusion and Outlook

Studying human metabolism guides the understanding of diverse diseases by determining the cells' health. The existence of high-quality genome-scale reconstructions facilitates systems-based insights into metabolism. As complex organisms, humans embody multiple cell and tissue types, each with different functions and metabolisms, leading to the essential use of cell- or tissue-specific metabolic networks to enable the accurate prediction of the cells' metabolic behavior. Here, we presented pymCADRE, a re-implementation of mCADRE[46] in Python that allows the reconstruction of tissue-specific human models based on human gene expression data and network topology information. Similar to the original mCADRE algorithm, pymCADRE consists of three parts: (1) ranking, (2) consistency check, and (3) pruning,

Preprints (www.preprints.org) | NOT PEER-REVIEWED | Posted: 27 July 2022 doi:10.20944/preprints202203.0290.v2

Table 3. Exemplary selection of already approved drugs that act against proteins associated with our predicted anti-SARS-CoV-2 target reactions and could possibly used for antiviral therapies. All listed drugs have known pharmacological action and are sorted based on the predicted percentage of virus reduction. NDPK1 with constrained fluxes resulted in considerable SARS-CoV-2 inhibition.

Reaction	EC-Number	Approved drug	Reference (PubMed ID)	Predicted % virus reduction
NDPK1	2.7.4.6	Acyclovir	7159465[58]	62.5
GK1	2.7.4.8	Acyclovir	1316735[59]	58.7
GRTTx	2.5.1.10	Ibandronate	11160603[60]	58.4
HMGCOARx	1.1.1.34	Lovastatin	1208255[61]	58.4

enabling the user to choose between two optimization methods, FVA and FASTCC, to check for model consistency. We enriched our implementations with data pre-processing scripts that simplify multiple data curation tasks.

We used our tool to create a tissue-specific model of the human bronchial epithelial cell (BEC1) to investigate SARS-CoV-2 infections. We used the human metabolic network Recon1 as a generic model to test our tool to avoid high computational costs. When FVA was used, pymCADRE proceeded faster than mCADRE, maintaining the highest possible similarity to the ground truth, i.e., the mCADRE-derived model. The two models showed a reaction overlap of almost 100 %, suggesting a substantial similarity between both implementations and demonstrating confidence about the quality of the pymCADRE models. Since we did not modify the initial mCADRE algorithm, the varying amount of reactions in the final tissue-specific models suggests variable performance among built-in functions in COBRAToolbox[66] and COBRApy[43]. More specifically, we observed divergent results among the two programming languages when FASTCC was employed. In both cases, the function is implemented as described by Vlassis *et al.*[67]; however the pythonic version detected a varying number of blocked reactions after multiple runs. The bug has already been reported and awaits resolve. Additionally, the detected inactive reactions were dissimilar compared to the reactions in the mCADRE model. This was not the case when the COBRApy methods,

```
flux_variability_analysis()
```

or

```
find_blocked_reactions()
```

from the package `cobra.flux_analysis` were employed. Moreover, the current version of FVA in MATLAB only supports the industrial proprietary CPLEX versions older than V 12.10[68]. The latest solver release, V 20.1 (released in December, 2020), does not yet include MATLAB-related binaries, and hence, FVA from the COBRAToolbox is of restricted use. This problem is resolved by pymCADRE, as the latest version of COBRApy enables the users to choose among the open-source GLPK package and the CPLEX solver from IBM to perform optimization tasks. Another reason for the divergent performance among both tools could be the implementation of organic exchange/demand reactions detection. We achieved this in a more powerful and fully automated script. Thus, pymCADRE detected four additional organic exchange/demand reactions in Recon1, affecting the result of consistency checks. The utilized human generic model, Recon1, does not include a BOF. We updated the generic human model by including a BOF extracted from the macrophage model published by Bordbar *et al.*[40].

Furthermore, we used our model and simulated an infection with the SARS-CoV-2 to better understand the host's impact on the virus and vice versa. For this purpose, we generated a SARS-CoV-2 VBOF based on the protocol of Aller *et al.* to create an integrated metabolic model aiming the analysis of host-virus interactions and the identification of effective targets for antiviral therapeutic strategies[10]. They recovered already known antiviral targets for the Chikungunya, Dengue, and Zika viruses within the human macrophage cell, verifying their approach's robustness. As Aller *et al.* suggested, FBA and FVA can be employed to predict essential host reactions, especially in cases of novel viruses. Two different computational experiments achieved this: single-reaction knock-outs and host-derived enforcement. Both approaches highlighted NDPK1 as a novel promising target to restrict the SARS-CoV-2 growth without harming the host. Among the detected targets, the already identified enzymatic target found for the macrophage and the lung models, GK1[27,52], was reported only by the host-derived enforcement. However, GK1 constrained, showed lower impact on the viral replication compared to NDPK1. Both NDPK1 and GK1 fall into the purine metabolism and are tightly coupled. This implies and verifies that drugs targeting the nucleotide metabolism exemplify a common therapeutic strategy to restrict SARS-CoV-2 replication. We conducted extensive literature and database search and found acyclovir as an already known inhibitor of both our targets from the purine synthesis pathway. So far, acyclovir is the standard gold treatment of infections with the herpes virus and the Varicella-Zoster Virus (VZV)[7,69]. In the context of SARS-CoV-2, acyclovir has been proposed in studies as a drug with an antiviral potential against coronaviruses[70], more specifically SARS-CoV-2 concurrently with signs of reactivation of VZV[71]. The authors assumed that this reacti-

Preprints (www.preprints.org) | NOT PEER-REVIEWED | Posted: 27 July 2022 doi:10.20944/preprints202203.0290.v2

vation is coupled to the unusually low count of lymphocytes (lymphopenia) in the COVID-19 patients' blood.

Besides that, we predicted lipids-related enzymatic candidate targets that involve cholesterol, phospholipids and sphingolipids. More specifically, most of the HDE-derived targets are located in the cholesterol metabolism, which has been reported to play a vital role upon SARS-CoV-2 infections. Lipids *per se* are essential in viral infections, as they are vital components of cellular and viral membranes. They regulate the viral fusion, replication, and release[72]. Besides that, lipids affect the host's metabolism to produce fatty acids for their own needs. It has been shown that suppression of fatty acid synthesis resulted in down-regulation of viral replication[73]. They have also been discussed in the literature to result in alterations of viral metabolic fluxes of SARS-CoV-2[29–31]. Engineering the cholesterol metabolism has been studied as an appealing therapeutic method in COVID-19 infections. The essential lipid cholesterol is found in cell membranes and plays an important role in controlling the conformations of transmembrane proteins and their fluidity. Like all lipids, cholesterol plays an important role in the initial stages of virus-host interactions by regulating the virus adherence to the cell membrane and its entry into the host cell[17,74,75]. From our reported targets, the enzyme SQLSr catalyzes the reaction that produces squalene, an intermediate in the biosynthesis of human steroids and direct precursor of cholesterol. Inhibiting SQLSr leads to lower levels of cholesterol. Moreover, inhibition of lanosterol synthase (LNSTLSr) has already been reported to remarkably suppress replication of Rhinovirus in primary normal human bronchial epithelial cells[76].

So far, statins have been widely used to prevent and treat cardiovascular diseases since they serve as lipid-lowering HMG-CoA reductase inhibitors. Statins suppress HMG-CoA, which is vital for cholesterol synthesis, leading to decreased levels of harmful low-density lipoproteins (LDL)[77]. Moreover, they have prevalent pleiotropic consequences, including anti-thrombotic, anti-inflammatory, and immune-regulatory effects[78]. Several studies have reported the direct relation of lipids, more specifically cholesterol, to the replication of the positive-sense single-stranded SARS-CoV and SARS-CoV-2[79–82]. With an extensive database search, we found available approved drugs, like lovastatin, simvastatin, atorvastatin, and rosuvastatin, with pharmacological action against our targets from the cholesterol metabolism. Reiner *et al*. showed that rosuvastatin and lovastatin could efficiently inhibit the main protease (M^{pro}) of SARS-CoV-2, a key enzyme in the replication machinery and proteolytic maturation[83]. Our literature search revealed studies that have already highlighted targeting the cholesterol metabolism using statins as an efficient treatment strategy against other single-stranded viruses. Glitscher *et al*. suggested novel cholesterol-regulating antivirals against the hepatitis E virus (HEV) that rely on the the increased viral release caused by decreased cholesterol levels[84]. Additionally, lovastatin has been studied in the context of the negative-sense single-stranded respiratory syncytial virus (RSV). Gower *et al*. confirmed the inhibitory effect of lovastatin *in vivo* and *in vitro* with respect to RSV infection[85]. Finally, a recent observational study based on a large population sample highlighted statins' negative correlation to the COVID-19 mortality[86].

Moreover, we tested two different growth media to validate the robustness of our predicted targets. GK1 was shown to be more effective against the virus with the blood medium defined, compared to the minimal defined medium. Using both media, NDPK1 demonstrated the same inhibitory effects, while diacylglycerol acyltransferase (DGAT) constrained within the blood medium showed a higher effect on virus replication. DGAT resulted as prominent hit target only after the incorporation of various lipids in the viral biomass composition. The inhibitory effect of DGAT has already been examined in the context of SARS-CoV-2[79,87,88]. These studies identified lipids, most specifically triacylglycerols, as inducers of SARS-CoV-2 metabolic dysregulation and highlighted DGAT as a potential antiviral target. Besides this, we observed that the chosen medium could strongly influence the resulting secondary metabolites, and this needs to be examined in more detail.

We further validated the robustness of our host-based targets against all five variants of concern (Alpha, Beta, Gamma, Delta, and Omicron). To accelerate the VBOF reconstruction, we developed PREDICATE to analyze multiple sequences for a single variant rapidly and in an automated way. Within this tool, we also implemented an algorithm to modify reference protein sequences and introduce amino acid mutations. Our implementations are transferable to all RNA viruses, as they are composed of the same building blocks. Firstly, we evaluated the mutations' effect on the computed stoichiometric coefficients variant-wise for the corresponding mutations. The high stoichiometric coefficients for ATP and ADP are consequences of decreased total viral molar masses and increased total amino acid counts. We observed increased use of lysine in the Omicron variant because most mutations replace amino acids with lysine. The opposite effect was observed in Omicron for asparagine. All single-reaction deletions across all variants highlighted NDPK1 as a potential robust antiviral inhibitor. The NDPK1 also proved by HDE to have the highest inhibitory effect against SARS-CoV-2, without harming the host cell. Besides that, supplementation of L-histidine, L-threonine, L-lysine, L-proline, and L-tryptophan in the host's environment shown to interrupt the virus's growth in all five SARS-CoV-2 variants.

Future improvements need to be done to make pymCADRE computationally feasible with more complex and more comprehensive models, including Recon2.2[89] and Recon3D[33]. Currently, pymCADRE and mCADRE need a great amount of computational time to complete the first part of the algorithm when a more complex generic model, like Recon3D, is used, which is the ranking of reactions. Both tools are automatically killed during pruning as there is no sufficient memory for them to process further reactions. However, we used Recon3D

Preprints (www.preprints.org) | NOT PEER-REVIEWED | Posted: 27 July 2022 doi:10.20944/preprints202203.0290.v2

to fill missing knowledge in our model Recon1-BEC1. Our targets' effectiveness needs to be verified in more updated networks that better represent the human metabolism. However, our integrated bronchial-specific metabolic model could be further expanded and investigated regarding the consequences of any upcoming mutation in the predicting antiviral targets. Models created by pymCADRE could be utilized to simulate the interaction of bacterial pathogens or symbionts and detect potential antiviral targets for drugs against emerging viruses on different host cells quickly. This new software provides the basis for systematic studies of a wide range of integrated computer models for host-pathogen interaction. It reduces the time for creating such models maintaining the highest possible similarity compared to the ground truth model. Our methods are based on the metabolic fluxes of infected cells and the interactions between the host cell and the virus. The latter remain unaffected by evolutionary changes. This, together with the fact that virus replication generally depends on conserved cellular pathways, drastically increases the likelihood of identifying druggable targets with broad antiviral activity. In addition, our predicted host-based targets are derived based on human patient data increasing thus their clinical relevance and their potential to achieve higher efficacy in COVID-19 therapies. Our database-derived drug compounds have already been suggested for other single-stranded RNA viruses, such as SARS-CoV-2, opening up the potential of experimentally verifying their safety, toxicity, and efficacy in cell culture experiments and in *in vitro* assays. Moreover, their optimum dosage and route of administration at different infection stages must be determined.

Altogether, we propose a complete workflow to create constraint-specific models and use them to predict host-based antiviral targets based on metabolic changes in infected cells. Our pipeline applies to RNA viruses that infect host cells, remarkably reduces the duration of target identification and compound selection, and accelerates the pre-clinical phase. Focusing on the metabolic changes of infected cells, we aim at applying our methods for rapid identification of potential antiviral targets to efficiently prevent future pandemics concerning various viruses and host cell types.

Materials and Methods

Overview of pymCADRE

The tool can be executed via the command line using:

```
python pymcadre.py
```

or using the provided Jupyter notebook named:

```
main_pymCADRE.ipynb
```

The package can also be found on the Python Package Index[90] (https://pypi.org/project/pymCADRE/) and can be installed using:

```
pip install pymcadre
```

Ranking of reactions

The first step in the pymCADRE pipeline is the ranking of all reactions found in the generic model, as Wang *et al.* proposed[46]. The ranking relies on three criteria: expression-based evidence, connectivity of reactions within the model, and confidence-based evidence. The assignment of evidence scores to reactions aims their division to cores and non-cores.

After binarizing the gene-expression data, the frequency of a gene's expression across all experiments of the same tissue is computed; this is the ubiquity score $U(g)$ for each gene g:

$$\forall g \in G : U(g) = \frac{1}{\mid N \mid} \sum_{n \in N} X_{g,n} \tag{1}$$

where N is the total number of samples and $X_{g,n} \in \{0,1\}$ denotes the absence or presence of the gene g in sample $n \in N$. For instance, if a gene is expressed in three of five samples, its ubiquity score will be 0.6. These scores are mapped to the corresponding reactions based on Gene-Protein-Reaction associationss (GPRs). That is the expression-based evidence $E_x(r)$ and can be either the minimum or maximum of two ubiquity scores depending on the respective GPRs rule: AND or OR. The expression-based evidence ranges from zero to one, indicating how likely a reaction is present in the selected tissue. More specifically, a score of zero represents a non-active reaction, while reactions with $E_x(r) > 0.9$ define the core set.

Afterwards, non-core reactions are ranked based on the connectivity-based evidence $E_c(r)$, using the network topology information of the generic model. This score defines in which order the reactions should be removed during pruning. The stoichiometric relationships in matrix $\mathbf{S}$ are applied to determine whether two reactions are connected. A pair of reactions are considered to be linked if they share at least one metabolite. For this purpose, a so-called weighted influence $WI(r)$ is calculated as the ratio between $E_x(r)$ and the outgoing influence of each reaction, i.e., the number of reactions connected to it. Then, the actual connectivity-based evidence is determined by the sum of the weighted influences of all reactions adjacent to reaction r. In Figure A11 we graphically illustrate the computation of each score using a toy metabolic network comprising six reactions and four genes coming from four samples. Lastly, the confidence level-based evidence $E_l(r)$ is the third measure of evidence for non-core reactions and indicates the level of biological evidence for the generic model.

Check Model Function

After classifying the reactions into cores and non-cores, pymCADRE tests the model's ability to produce key metabolites from glucose. These include compounds in the TCA and glycolysis, non-essential amino acids, and more. Totally, 38 metabolites were tested based on previously described criteria and used to evaluate similar models by the authors of mCADRE[46]. This list can be expanded and modified utilizing metabolomics data to include tissue-specific metabolites or known abilities of the tissue of interest.

Preprints (www.preprints.org) | NOT PEER-REVIEWED | Posted: 27 July 2022 doi:10.20944/preprints202203.0290.v2

Model Pruning

The last step of pymCADRE is to sequentially remove each non-core reaction in a reversed order, i.e., beginning from those with the lowest calculated evidence[46]. The respective reaction will be removed if, and only if, its elimination does not prevent the model from producing key metabolites and the set of core reactions remains consistent. This consistency is tested by determining each reaction's minimum and maximum flux while ensuring that at least one is zero.

More specifically, firstly, the production of precursor metabolites is checked. If this test fails, there is no need to check for model consistency with FVA or FASTCC (time-saving step). If the test leads to successful results, the set of inactive cores and non-cores is determined, and the algorithm moves on with the removal of reactions. Reactions with zero expression will be removed with their corresponding inactive core reactions if sufficiently more non-cores are pruned. On the other hand, if the reaction has expression evidence, pymCADRE only attempts to remove inactive non-cores.

Integration of transcriptomic data in a human genome-scale metabolic model

The functionality of pymCADRE was tested using gene expression data of human bronchial epithelial cell (BEC1) downloaded from the Gene Expression Omnibus (GEO) database (accession number: `GSE3397`)[91]. The derived experimental data was generated using the `GPL570` microarray platform and contained four control samples, each with 54,675 experiments[92]. Each sample file encompasses information about the probeset ID, the average intensity of probe intensities for a specific gene, and an absolute call value (i.e., P = present, A = absent, and M = on the borderline detection), which indicates whether messenger Ribonucleic Acid (mRNA) has been detected for that specific gene or not, meaning whether it is expressed or not. All data obtained from GEO underwent manual curation and pre-treatment with scripts that we provided together with the pymCADRE source code. The first curation step involved collecting confidence scores from the Virtual Metabolic Human (VMH) database, assigned to all reactions in the model. Then, the raw sample transcriptomic data was enhanced with two new information, gene symbol and Entrez identifiers. During binarization, genes present in the sample took the value of one, while marginal and absent calls were assigned to zero. Lastly, the essential ubiquity scores were calculated to represent a single gene's expression frequency across all samples.

The literature-based Recon1[32] was obtained from the BiGG database[93] and was used as a generic host human model. It consists of 3,741 reactions, 2,766 metabolites, 1,905 transcripts, and 1,497 unique genes. We also incorporated a BOF to Recon1 since it does not include one. For this purpose, we used the objective function from the human alveolar macrophage model published by Bordbar *et al.* in 2010[40]. The biomass reaction with the identifier `biomass_bec` represents the cellular maintenance requirements such as the ATP maintenance.

In the Recon1 model, there is no constraint growth medium defined; thus, all extracellular transport reactions have a minimum flux value of $-1{,}000.0\,\mathrm{mmol}/(\mathrm{gDW}\cdot\mathrm{h})$. This means that all exchanges are allowed to carry a flux (rich medium), resulting to unusually high cell growth rates. We have defined here a minimal growth medium using the COBRApy built-in function[43], which contains only essential components for growth. Since the availability of nutrients has a major impact on the metabolic fluxes, we re-ran our simulations using the blood medium[53]. The exact compositions of both media are provided in the supplementary file S3.

We manually expanded our model by adding missing exchange reactions to all extracellular metabolites. We also updated all reaction annotations in our tissue-specific model, Recon1-BEC1, by assigning KEGG IDs[44] and retrieving the corresponding pathways using the KEGG Representational State Transfer (REST) Application Programming transfer Interface (API). These subsystems were incorporated into the model as additional annotations to each reaction with the biological qualifier type `BQB_OCCURS_IN`. The reaction pathways were merged into main classes based on the KEGG classification system (`https://www.kegg.jp/kegg/pathway.html`). Additionally to the functionality checks incorporated into the mCADRE and consequently into pymCADRE, we examined the presence of futile cycles in our final tissue-specific model. As Fritzemeier *et al.* proposed, we tested the production of energy-generating compounds by including energy dissipation reactions and disabling the external uptake of all metabolites[47]. Our final model could not produce any of the tested metabolites, meaning no futile cycles were included. The test compounds are listed in the supplementary file S0.

The reconstructions were conducted using a 3.3 GHz processor and 16 GB RAM, while MEMOTE[51] and the SBML Validator from the libSBML[50] were employed to assess the model's quality.

Stoichiometric reconstruction of SARS-CoV-2 biomass objective function

Similar to the biomass production function used for microbial metabolic models, the VBOF is a single pseudo-reaction imitating the production of different virus particles. It consists of nucleotides, amino acids, and components necessary for energy supply. The SARS-CoV-2 virus biomass objective function was created as proposed by Aller *et al.*[10] and as extended by Renz *et al.*[52]. The approach considers the viral structure and its genome sequence, the subsequently encoded proteins, and their copy number, as well as the energy requirements for nucleotide and peptide bonds[10]. The viral genome and protein sequences were downloaded from the National Centre for Biotechnology Information (NCBI) nucleotide database[94] (accession number: `NC_045512.2`, accessed in May, 2020). The genome copy number (G_g) and the number of copies of each of the non-structural proteins (C_{np}) was assumed to be

one[10]. Moreover, the copy number of structural proteins was set to 1,000 for membrane proteins (C_m), 456 for nucleocapsid phosphoproteins (C_n), 120 for spike proteins (C_s), and 20 for envelope proteins (C_e)[52].

The SARS-CoV-2 falls into the fourth Baltimore group of viruses (Group IV, positive-sense single-stranded RNA viruses)[95], i.e., it synthesizes mRNA with the help of a template "-" single RNA antisense strand. Thus, the count of nucleotides in the positive strand equals the number of nucleotides in the complementary negative strand. The total moles of each nucleotide in a mole of virus particle were obtained by summing up the nucleotides in the positive and negative strand and multiplying this by the genome copy number. The moles were then converted into grams of nucleotide per mole of the virus by multiplying them with the respective molar mass of the nucleotides[10]. Similar calculations were conducted for the amino acids, as well. Eventually, the stoichiometric coefficients of each nucleotide and amino acid in the VBOF were calculated using the total viral molar mass[10].

For the estimation of the energetic requirements, the ATP requirement per amino acid polymerization and the pyrophosphate liberation during the polymerization of nucleotide monomers were considered. As proposed by Aller *et al.*, four ATP molecules and one pyrophosphate molecule are participating in the formation of nucleotide and amino acid polymers, respectively[10]. Subsequently, the total molar mass of the virus was calculated as the sum of all genome and proteome components.

Finally, to account for the lipid requirements we included phosphatidylcholine (`pchol_hs_c`), phosphatidylethanolamine (`pe_hs_c`), phosphatidylinositol (`pail_hs_c`), phosphatidylserine (`ps_hs_c`), cholesterol (`chsterol_c`), and sphingomyelin (`sphmyln_hs_c`) into the viral biomass function. Renz *et al*. examined the influence of lipids with various stoichiometric coefficients in the viral biomass function and the prediction of antiviral targets. However, they did not incorporated the lipid composition of a single virion into their final viral function[26]. Thus, we computed stoichiometric coefficients for these lipids from the surface area of a virion as suggested by Nanda *et al*.[28].

The generated final VBOF was appended into Recon1-BEC1, with a lower bound of zero and an upper bound of 1,000. The individual VBOF components and their stoichiometric coefficients are listed in Table A4.

Prediction of host-based antiviral targets

Subsequent analysis of Recon1-BEC1 allowed us to identify metabolic targets for antiviral therapies. As proposed by Aller *et al*., FBA and FVA can be used to predict essential host reactions, especially in cases of novel emerging viruses[10]. This can be computationally achieved in two different ways: via single knock-out analysis or via HDE.

The single-reaction knock-out analysis investigates the effect of individual reactions with no flux. Both lower and upper bounds were systematically set to zero once with BOF as the objective function and once with the VBOF. Metabolic targets were reported when the host growth rate was higher than the virus growth rate and when more than 99 % of the initial host growth rate was maintained.

A less harmful approach for the cell is the host-derived enforcement. As Aller *et al*. suggested, herein method, the reaction fluxes are constraint to FVA-derived ranges so that the maintenance of the optimal host state is achieved while reducing the virus propagation. For our analysis, we used an updated version of this method as modified by Renz *et al*.[52]. The re-calculated flux ranges for every reaction were then utilized, and the model was optimized for the VBOF. The resulting optima for the virus production were compared to the original optimal value. Hence, potential antiviral targets were reported when the virus growth rate with altered bounds was beneath the threshold of 50 % of the initial growth rate. Additionally, to ensure a reduction of the virus replication, we keep only targets that had a non-zero flux when the VBOF was optimized. Our Recon1-BEC1 model was examined for potential antiviral targets using both methods.

Testing targets' robustness against all known variants of concern

To test our targets' robustness, we examined the consequences of concerning SARS-CoV-2 mutations on our predicted metabolic targets. As of February, 2022, five SARS-CoV-2 VOC are known to differ from the conventional virus in terms of their pathogen properties (e.g., transferability, virulence, or susceptibility to the immune response of recovered or vaccinated people). These are the Alpha, Beta, Gamma, Delta, and Omicron variants[19]. Genomic sequences of patients infected with SARS-CoV-2 were retrieved from the GISAID's EpiCoV™ database[56]. For each variant, we randomly selected 20 sequences adjusting only the location and variants filters as follows: (i) Europe/United Kingdom for VOC Alpha GRY (B.1.1.7+Q.*), (ii) Africa/South Africa for VOC Beta GH/501Y.V2 (B.1.351+B.1.351.2+B.1.351.3), (iii) South America/Brazil for VOC Gamma GR/501Y.V3 (P.1+P.1.*), (iv) Asia/India for VOC Delta GK (B.1.617.2+AY.*), and (v) Africa/Botswana and Africa/South Africa for VOC Omicron GRA (B.1.1.529). We investigated 100 sample sequences in total. To calculate the amino acid investment per virus, we used the annotated protein sequence of the SARS-CoV-2 reference genome (NCBI accession: `NC_045512.2`) and the mutation information extracted from GISAID. All used datasets and tested mutations are provided in the supplementary material S2.

We calculated the stoichiometric coefficients of growth-related constituents for each mutated sequence and reconstructed for each one a VBOF as described in the previous sections. To speed up the calculations, we implemented PREDICATE, an automated script, which takes as input one or more genome sequences and computes the metabolic stoichiometry using information from the viral genome, the encoded

proteins and their copy numbers, and the energetic requirements (Figure 7). The amino acid coefficients are calculated using the reference protein sequence, which our algorithm mutates by introducing all reported mutations (replacements, insertions, deletions, and duplications) extracted from the metadata. Afterwards, each VBOF is integrated into a given cell-specific metabolic network, in our study Recon1-BEC1, to create a host-virus model. Lastly, PREDICATE applies single-reaction knock-outs and HDE to the integrated model resulting in experimentally testable and robust metabolic virus-suppressing targets. Our script also generates different plots, providing insights into the dataset and a better understanding of the results. To evaluate the mutations' effect on the viral biomass, we computed the mean of all estimated coefficients across all mutated sequences and compared them against the WT coefficients.

PREDICATE can be applied to either one or more nucleotide sequences and all existing RNA viruses. This makes it particularly advantageous and time-saving to simultaneously study multiple viruses and variants.

Data and Code availability

The computational host-virus model Recon1-BEC1, as well as the source code of pymCADRE, test scripts, test dataset, and a script to create VBOF and predict enzymatic host-based targets are available in a git repository at https://github.com/draeger-lab/pymCADRE/. Supplementary tables in Microsoft Excel format are available along with this article. The SBML model[96,97] of the SARS-CoV-2-infected bronchial epithelial cell is available at the BioModels Database[98] as an SBML Level 3 Version 2 file[48] distributed as Open Modeling EXchange format (OMEX) archive[99]. Access the model at https://www.ebi.ac.uk/biomodels/MODEL2202240001.

Acknowledgments

This work was funded by Federal Ministry of Education and Research (BMBF) and the Baden-Württemberg Ministry of Science as part of the Excellence Strategy of the German Federal and State Governments within the project "identification of robust antiviral drug targets against SARS-CoV-2" as well as by the *Deutsche Forschungsgemeinschaft* (DFG, German Research Foundation) under Germany's Excellence Strategy – EXC 2124 – 390838134 and supported by the Cluster of Excellence 'Controlling Microbes to Fight Infections' (CMFI). A.D. is supported by the German Center for Infection Research (DZIF, doi: 10.13039/100009139) within the *Deutsche Zentren der Gesundheitsforschung* (BMBF-DZG, German Centers for Health Research of the BMBF), grant № 8020708703. The authors acknowledge the use of de.NBI cloud and the support by the High Performance and Cloud Computing Group at the *Zentrum für Datenverarbeitung* (ZDV) of the University of Tübingen and the BMBF through grant № 031 A535A. The authors acknowledge the support by the Open Access Publishing Fund of the University of Tübingen (https://uni-tuebingen.de/en/216529). The authors also thank the reviewers for their valuable comments to improve the manuscript.

Author contributions

N.L. developed the software tools, collected the data, performed the analyses, and wrote the manuscript under guidance of A.R., R.M., and A.D. A.D. supervised the study and finalized the manuscript with N.L. All authors approved the publishing of the manuscript.

Competing interests:

The authors declare no conflict of interest.

List of Abbreviations

dGTP	deoxyguanosine triphosphate
mCADRE	metabolic Context-specificity Assessed by Deterministic Reaction Evaluation
mRNA	messenger Ribonucleic Acid
ADP	Adenosine Diphosphate
API	Application Programming transfer Interface
ATP	Adenosine Triphosphate
BEC1	human bronchial epithelial cell
BiGG	Biochemcial, Genetical, and Genomical
BMBF	Federal Ministry of Education and Research (*Bundesministerium für Bildung und Forschung*)
BMBF-DZG	*Deutsche Zentren der Gesundheitsforschung*
BOF	Biomass Objective Function
BRENDA	Brunswick Enzyme Database
CMFI	Controlling Microbes to Fight Infections
COBRApy	Constraints-Based Reconstruction and Analysis for Python
COVID-19	Coronavirus Disease 2019
DFG	*Deutsche Forschungsgemeinschaft*
DNA	Deoxyribonucleic Acid
DZIF	German Center for Infection Research
EC	Enzyme Commission
EDA	Explanatory Data Analysis
ExoN	exonuclease
FBA	Flux Balance Analysis
FVA	Flux Variability Analysis
GDP	Guanosine Diphosphate
GEM	Genome-scale Metabolic Model
GEO	Gene Expression Omnibus
GISAID	Global Initiative on Sharing All Influenza Data
GK1	Guanylate Kinase
GPR	Gene-Protein-Reaction associations
GTP	Guanosine Triphosphate

HDE	host-derived enforcement
HEV	hepatitis E virus
ID	identifier
KEGG	Kyoto Encyclopedia of Genes and Genomes
MEMOTE	Metabolic Model Testing
NCBI	National Centre for Biotechnology Information
NDPK1	Nucleoside Diphosphate Kinase
NSP	non-structural protein
NSP14	non-structural protein 14
OMEX	Open Modeling EXchange format
PREDICATE	Prediction of Antiviral Targets
RAM	random-access memory
RNA	Ribonucleic Acid
REST	Representational State Transfer
RSV	respiratory syncytial virus
SARS	Severe Acute Respiratory Syndrome
SARS-CoV	Severe Acute Respiratory Syndrome Coronavirus
SARS-CoV-2	Severe Acute Respiratory Syndrome Coronavirus 2
SBFC	Systems Biology Format Converter
SBML	Systems Biology Markup Language
TCA	Tricarboxylic Acid Cycle
VMH	Virtual Metabolic Human
VBOF	Virus Biomass Objective Function
VOC	variants of concern
VZV	Varicella-Zoster Virus
WHO	World Health Organization
WT	Wildtype
ZDV	*Zentrum für Datenverarbeitung* (Center for Data Processing)

References

1. Cheng, V. C., Lau, S. K., Woo, P. C. & Yuen, K. Y. Severe acute respiratory syndrome coronavirus as an agent of emerging and reemerging infection. *Clin. microbiology reviews* **20**, 660–694, DOI: 10.1128/CMR.00023-07 (2007).
2. Taubenberger, J. K. & Morens, D. M. 1918 Influenza: the mother of all pandemics. *Revista Biomed.* **17**, 69–79, DOI: 10.3201/eid1201.050979 (2006).
3. Ryu, W.-S. Part III. RNA Viruses. In Ryu, W.-S. (ed.) *Molecular Virology of Human Pathogenic Viruses*, 149–150, DOI: https://doi.org/10.1016/B978-0-12-800838-6.00044-8 (Academic Press, Boston, 2017).
4. Maynard, N. D., Gutschow, M. V., Birch, E. W. & Covert, M. W. The virus as metabolic engineer. *Biotechnol. journal* **5**, 686–694, DOI: 10.1002/biot.201000080 (2010).
5. Leyssen, P., De Clercq, E. & Neyts, J. Molecular strategies to inhibit the replication of RNA viruses. *Antivir. research* **78**, 9–25, DOI: 10.1016/j.antiviral.2008.01.004 (2008).
6. Feld, J. J. & Hoofnagle, J. H. Mechanism of action of interferon and ribavirin in treatment of hepatitis C. *Nature* **436**, 967–972, DOI: 10.1038/nature04082 (2005).
7. Engel, J. P., Englund, J. A., Fletcher, C. V. & Hill, E. L. Treatment of resistant herpes simplex virus with continuous-infusion acyclovir. *Jama* **263**, 1662–1664 (1990).
8. Warren, T. K. *et al.* Therapeutic efficacy of the small molecule GS-5734 against Ebola virus in rhesus monkeys. *Nature* **531**, 381–385 (2016).
9. Maynard, N. D. *et al.* A forward-genetic screen and dynamic analysis of lambda phage host-dependencies reveals an extensive interaction network and a new antiviral strategy. *PLoS genetics* **6**, e1001017, DOI: 10.1038/nature17180 (2010).
10. Aller, S., Scott, A., Sarkar-Tyson, M. & Soyer, O. S. Integrated human-virus metabolic stoichiometric modelling predicts host-based antiviral targets against Chikungunya, Dengue and Zika viruses. *J. The Royal Soc. Interface* **15**, 20180125, DOI: 10.1098/rsif.2018.0125 (2018).
11. Smith, E. C. The not-so-infinite malleability of RNA viruses: Viral and cellular determinants of RNA virus mutation rates. *PLoS pathogens* **13**, e1006254, DOI: 10.1371/journal.ppat.1006254 (2017).
12. Drake, J. W. Rates of spontaneous mutation among RNA viruses. *Proc. Natl. Acad. Sci.* **90**, 4171–4175, DOI: 10.1073/pnas.90.9.4171 (1993).
13. Bar-On, Y. M., Flamholz, A., Phillips, R. & Milo, R. Science Forum: SARS-CoV-2 (COVID-19) by the numbers. *elife* **9**, e57309, DOI: 10.7554/eLife.57309 (2020).
14. Domingo, E. & Holland, J. RNA virus mutations and fitness for survival. *Annu. review microbiology* **51**, 151–178, DOI: 10.1146/annurev.micro.51.1.151 (1997).
15. Robson, F. *et al.* Coronavirus RNA Proofreading: Molecular Basis and Therapeutic Targeting. *Mol. cell* **79**, 710–727, DOI: 10.1016/j.molcel.2020.07.027 (2020).
16. Moeller, N. H. *et al.* Structure and dynamics of SARS-CoV-2 proofreading exoribonuclease ExoN. *bioRxiv* DOI: 10.1073/pnas.2106379119 (2021).
17. Chan, R. B., Tanner, L. & Wenk, M. R. Implications for lipids during replication of enveloped viruses. *Chem. physics lipids* **163**, 449–459, DOI: 0.1016/j.chemphyslip.2010.03.002 (2010).
18. Kim, D. *et al.* The architecture of SARS-CoV-2 transcriptome. *Cell* **181**, 914–921, DOI: 10.1016/j.cell.2020.04.011 (2020).

19. World Health Organization. Covid-19 weekly epidemiological update 76– 25 january 2022. Accessed on February 8, 2022.

20. Korber, B. *et al.* Tracking changes in SARS-CoV-2 spike: evidence that D614G increases infectivity of the COVID-19 virus. *Cell* **182**, 812–827, DOI: 10.1016/j.cell.2020.06.043 (2020).

21. Timmers, L. F. S. M. *et al.* SARS-CoV-2 mutations in Brazil: from genomics to putative clinical conditions. *Sci. reports* **11**, 1–14, DOI: 10.1038/s41598-021-91585-6 (2021).

22. Kannan, S. R. *et al.* Omicron SARS-CoV-2 variant: Unique features and their impact on pre-existing antibodies. *J. autoimmunity* **126**, 102779, DOI: 10.1016/j.jaut.2021.102779 (2022).

23. Becker, S. A. & Palsson, B. O. Context-specific metabolic networks are consistent with experiments. *PLoS computational biology* **4**, e1000082, DOI: 10.1371/journal.pcbi.1000082 (2008).

24. Uhlén, M. *et al.* Proteomics. Tissue-based map of the human proteome. *Science* **347**, DOI: 10.1126/science.1260419 (2015).

25. Mayer, K. A., Stöckl, J., Zlabinger, G. J. & Gualdoni, G. A. Hijacking the supplies: metabolism as a novel facet of virus-host interaction. *Front. immunology* 1533 (2019).

26. Renz, A., Widerspick, L. & Dräger, A. FBA reveals guanylate kinase as a potential target for antiviral therapies against SARS-CoV-2. *Bioinformatics* **36**, i813–i821, DOI: 10.1093/bioinformatics/btaa813 (2020).

27. Delattre, H., Sasidharan, K. & Soyer, O. S. Inhibiting the reproduction of SARS-CoV-2 through perturbations in human lung cell metabolic network. *Life science alliance* **4**, DOI: 10.26508/lsa.202000869 (2021).

28. Nanda, P. & Ghosh, A. Genome scale-differential flux analysis reveals deregulation of lung cell metabolism on sars-cov-2 infection. *PLoS computational biology* **17**, e1008860 (2021).

29. Cheng, K. *et al.* Genome-scale metabolic modeling reveals sars-cov-2-induced metabolic changes and antiviral targets. *Mol. systems biology* **17**, e10260 (2021).

30. Bannerman, B. P. *et al.* Integrated human/SARS-CoV-2 metabolic models present novel treatment strategies against COVID-19. *Life science alliance* **4**, DOI: 10.26508/lsa.202000954 (2021).

31. Kishk, A., Pacheco, M. P. & Sauter, T. Dccov: Repositioning of drugs and drug combinations for sars-cov-2 infected lung through constraint-based modeling. *Iscience* **24**, 103331 (2021).

32. Duarte, N. C. *et al.* Global reconstruction of the human metabolic network based on genomic and bibliomic data. *Proc. Natl. Acad. Sci.* **104**, 1777–1782, DOI: 10.1073/pnas.0610772104 (2007).

33. Brunk, E. *et al.* Recon3D enables a three-dimensional view of gene variation in human metabolism. *Nat. Biotechnol.* **36**, 272–281 (2018).

34. MATLAB. *version R2020a* (The MathWorks Inc., Natick, Massachusetts, 2020).

35. Liao, M. *et al.* Single-cell landscape of bronchoalveolar immune cells in patients with COVID-19. *Nat. medicine* **26**, 842–844, DOI: 10.1038/s41591-020-0901-9 (2020).

36. Tian, S. *et al.* Pathological study of the 2019 novel coronavirus disease (COVID-19) through postmortem core biopsies. *Mod. Pathol.* **33**, 1007–1014, DOI: 10.1038/s41379-020-0536-x (2020).

37. Kam, Y.-W. *et al.* Cleavage of the SARS coronavirus spike glycoprotein by airway proteases enhances virus entry into human bronchial epithelial cells in vitro. *PloS one* **4**, e7870, DOI: 10.1371/journal.pone.0007870 (2009).

38. Chua, R. L. *et al.* COVID-19 severity correlates with airway epithelium–immune cell interactions identified by single-cell analysis. *Nat. biotechnology* **38**, 970–979, DOI: 10.1038/s41587-020-0602-4 (2020).

39. Ravindra, N. G. *et al.* Single-cell longitudinal analysis of SARS-CoV-2 infection in human airway epithelium identifies target cells, alterations in gene expression, and cell state changes. *PLoS biology* **19**, e3001143, DOI: 10.1371/journal.pbio.3001143 (2021).

40. Bordbar, A., Lewis, N. E., Schellenberger, J., Palsson, B. Ø. & Jamshidi, N. Insight into human alveolar macrophage and M. tuberculosis interactions via metabolic reconstructions. *Mol. systems biology* **6**, 422, DOI: 10.1038/msb.2010.68 (2010).

41. Jeske, L., Placzek, S., Schomburg, I., Chang, A. & Schomburg, D. BRENDA in 2019: a European ELIXIR core data resource. *Nucleic acids research* **47**, D542–D549, DOI: 10.1093/nar/gky1048 (2019).

42. Wishart, D. S. *et al.* DrugBank: a comprehensive resource for in silico drug discovery and exploration. *Nucleic acids research* **34**, D668–D672, DOI: 10.1093/nar/gkj067 (2006).

43. Ebrahim, A., Lerman, J. A., Palsson, B. O. & Hyduke, D. R. COBRApy: constraints-based reconstruction and analysis for python. *BMC systems biology* **7**, 1–6, DOI: 10.1186/1752-0509-7-74 (2013).

44. Kanehisa, M., Sato, Y. & Kawashima, M. KEGG mapping tools for uncovering hidden features in biological data. *Protein Sci.* DOI: 10.1002/pro.4172 (2021).

45. Romero, P. *et al.* Computational prediction of human metabolic pathways from the complete human genome. *Genome biology* **6**, 1–17 (2005).

46. Wang, Y., Eddy, J. A. & Price, N. D. Reconstruction of genome-scale metabolic models for 126 human tissues using mCADRE. *BMC systems biology* **6**, 1–16, DOI: 10.1186/1752-0509-6-153 (2012).

47. Fritzemeier, C. J., Hartleb, D., Szappanos, B., Papp, B. & Lercher, M. J. Erroneous energy-generating cycles in published genome scale metabolic networks: Identification and removal. *PLoS computational biology* **13**, e1005494, DOI: 10.1371/journal.pcbi.1005494 (2017).

48. Hucka, M. *et al.* Systems Biology Markup Language (SBML): Language Specification for Level 3 Version 2 Core Release 2. *J. Integr. Bioinforma.* **16**, 1, DOI: 10.1515/jib-2019-0021 (2019).

49. Rodriguez, N. *et al.* The systems biology format converter. *BMC bioinformatics* **17**, 1–7, DOI: 10.1186/s12859-016-1000-2 (2016).

50. Bornstein, B. J., Keating, S. M., Jouraku, A. & Hucka, M. LibSBML: an API library for SBML. *Bioinformatics* **24**, 880–881, DOI: 10.1093/bioinformatics/btn051 (2008).

51. Lieven, C. *et al.* MEMOTE for standardized genome-scale metabolic model testing. *Nat. biotechnology* **38**, 272–276, DOI: 10.1038/s41587-020-0446-y (2020).

52. Renz, A., Widerspick, L. & Dräger, A. Genome-Scale Metabolic Model of Infection with SARS-CoV-2 Mutants Confirms Guanylate Kinase as Robust Potential Antiviral Target. *Genes* **12**, DOI: 10.3390/genes12060796 (2021).

53. Bernardes, J. P. *et al.* Longitudinal multi-omics analyses identify responses of megakaryocytes, erythroid cells, and plasmablasts as hallmarks of severe COVID-19. *Immunity* **53**, 1296–1314, DOI: 10.1016/j.immuni.2020.11.017 (2020).

54. Touré, V., Dräger, A., Luna, A., Dogrusoz, U. & Rougny, A. The Systems Biology Graphical Notation: Current Status and Applications in Systems Medicine. In Wolkenhauer, O. (ed.) *Systems Medicine*, vol. 3, 372–381, DOI: 10.1016/B978-0-12-801238-3.11515-6 (Academic Press, Oxford, 2020).

55. Balcı, H. *et al.* Newt: a comprehensive web-based tool for viewing, constructing and analyzing biological maps. *Bioinformatics* **37**, 1475–1477, DOI: 10.1093/bioinformatics/btaa850 (2021).

56. Khare, S. *et al.* GISAID's Role in Pandemic Response. *China CDC Wkly.* **3**, 1049, DOI: 10.46234/ccdcw2021.255 (2021).

57. Kumar, S., Thambiraja, T. S., Karuppanan, K. & Subramaniam, G. Omicron and Delta variant of SARS-CoV-2: A comparative computational study of spike protein. *J. medical virology* DOI: 10.1002/jmv.27526 (2021).

58. Miller, W. H. & Miller, R. L. Phosphorylation of acyclovir diphosphate by cellular enzymes. *Biochem. pharmacology* **31**, 3879–3884, DOI: 10.1016/0006-2952(82)90305-7 (1982).

59. O'Brien, J. J. & Campoli-Richards, D. M. Acyclovir. *Drugs* **37**, 233–309 (1989).

60. Dunford, J. E. *et al.* Structure-activity relationships for inhibition of farnesyl diphosphate synthase in vitro and inhibition of bone resorption in vivo by nitrogen-containing bisphosphonates. *J. Pharmacol. Exp. Ther.* **296**, 235–242 (2001).

61. Dimitroulakos, J. *et al.* Microarray and biochemical analysis of lovastatin-induced apoptosis of squamous cell carcinomas. *Neoplasia* **4**, 337–346, DOI: 10.1038/sj.neo.7900247 (2002).

62. Elion, G. B. Mechanism of action and selectivity of acyclovir. *The Am. journal medicine* **73**, 7–13, DOI: 10.1016/0002-9343(82)90055-9 (1982).

63. Whitley, R. J. & Gnann Jr, J. W. Acyclovir: a decade later. *New Engl. J. Medicine* **327**, 782–789, DOI: 10.1056/NEJM199209103271108 (1992).

64. Tong, X. *et al.* Merimepodib, an IMPDH inhibitor, suppresses replication of Zika virus and other emerging viral pathogens. *Antivir. research* **149**, 34–40, DOI: 10.1016/j.antiviral.2017.11.004 (2018).

65. Ortiz-Riaño, E. *et al.* Inhibition of arenavirus by A3, a pyrimidine biosynthesis inhibitor. *J. virology* **88**, 878–889, DOI: 10.1128/JVI.02275-13 (2014).

66. Heirendt, L. *et al.* Creation and analysis of biochemical constraint-based models using the COBRA Toolbox v. 3.0. *Nat. protocols* **14**, 639–702, DOI: 10.1038/s41596-018-0098-2 (2019).

67. Vlassis, N., Pacheco, M. P. & Sauter, T. Fast reconstruction of compact context-specific metabolic network models. *PLoS computational biology* **10**, e1003424, DOI: 10.1371/journal.pcbi.1003424 (2014).

68. Cplex, I. I. V12. 1: User's Manual for CPLEX. *Int. Bus. Mach. Corp.* **46**, 157 (2009).

69. Balfour Jr, H. H., McMonigal, K. A. & Bean, B. Acyclovir therapy of varicella-zoster virus infections in immunocompromised patients. *J. Antimicrob. Chemother.* **12**, 169–179, DOI: 10.1093/jac/12.suppl_b.169 (1983).

70. Tan, E. L. *et al.* Inhibition of SARS coronavirus infection in vitro with clinically approved antiviral drugs. *Emerg. infectious diseases* **10**, 581, DOI: 10.3201/eid1004.030458 (2004).

71. Nofal, A., Fawzy, M. M., Deen, S. M. S. E. & El-Hawary, E. E. Herpes zoster ophthalmicus in COVID-19 patients. *Int. J. Dermatol.* **59**, 1545, DOI: 10.1111/ijd.15240 (2020).

72. Lorizate, M. & Kräusslich, H.-G. Role of lipids in virus replication. *Cold Spring Harb. perspectives biology* **3**, a004820, DOI: 10.1101/cshperspect.a004820 (2011).

73. Sanchez, E. L. & Lagunoff, M. Viral activation of cellular metabolism. *Virology* **479**, 609–618, DOI: 10.1016/j.virol.2015.02.038 (2015).

74. Wei, C. *et al.* HDL-scavenger receptor B type 1 facilitates SARS-CoV-2 entry. *Nat. metabolism* **2**, 1391–1400, DOI: 10.1038/s42255-020-00324-0 (2020).

75. Wang, S. *et al.* Cholesterol 25-Hydroxylase inhibits SARS-CoV-2 and other coronaviruses by depleting membrane cholesterol. *The EMBO journal* **39**, e106057, DOI: 10.15252/embj.2020106057 (2020).

76. McCrae, C. *et al.* Lanosterol synthase regulates human rhinovirus replication in human bronchial epithelial cells. *Am. J. Respir. Cell Mol. Biol.* **59**, 713–722 (2018).

77. Kostner, G. M. *et al.* HMG CoA reductase inhibitors lower LDL cholesterol without reducing Lp (a) levels. *Circulation* **80**, 1313–1319, DOI: 10.1161/01.cir.80.5.1313 (1989).

78. Liao, J. K. & Laufs, U. Pleiotropic effects of statins. *Annu. Rev. Pharmacol. Toxicol.* **45**, 89–118, DOI: 10.1146/annurev.pharmtox.45.120403.095748 (2005).

79. Dias, S. S. G. *et al.* Lipid droplets fuel SARS-CoV-2 replication and production of inflammatory mediators. *PLoS pathogens* **16**, e1009127, DOI: 10.1371/journal.ppat.1009127 (2020).

80. Nardacci, R. *et al.* Evidences for lipid involvement in SARS-CoV-2 cytopathogenesis. *Cell death & disease* **12**, 1–12, DOI: 10.1038/s41419-021-03527-9 (2021).

81. Wei, X. *et al.* Hypolipidemia is associated with the severity of COVID-19. *J. clinical lipidology* **14**, 297–304, DOI: HypolipidemiaisassociatedwiththeseverityofCOVID-19 (2020).

82. Hu, X., Chen, D., Wu, L., He, G. & Ye, W. Declined serum high density lipoprotein cholesterol is associated with the severity of COVID-19 infection. *China (November 21, 2020)* DOI: 10.1016/j.cca.2020.07.015 (2020).

83. Reiner, Ž. *et al.* Statins and the COVID-19 main protease: in silico evidence on direct interaction. *Arch. medical science: AMS* **16**, 490, DOI: 10.5114/aoms.2020.94655 (2020).

84. Glitscher, M. *et al.* Targeting cholesterol metabolism as efficient antiviral strategy against the hepatitis E Virus. *Cell. Mol. Gastroenterol. Hepatol.* **12**, 159–180, DOI: 10.1016/j.jcmgh.2021.02.002 (2021).

85. Gower, T. L. & Graham, B. S. Antiviral activity of lovastatin against respiratory syncytial virus in vivo and in vitro. *Antimicrob. agents chemotherapy* **45**, 1231–1237, DOI: 10.1128/AAC.45.4.1231-1237.2001 (2001).

86. Bergqvist, R. *et al.* HMG-CoA reductase inhibitors and COVID-19 mortality in Stockholm, Sweden: A registry-based cohort study. *PLoS medicine* **18**, e1003820, DOI: ournal.pmed.1003820 (2021).

87. Williams, C. G. *et al.* Inhibitors of vps34 and fatty-acid metabolism suppress sars-cov-2 replication. *Cell Reports* **36**, 109479 (2021).

88. Yuan, S. *et al.* Sars-cov-2 exploits host dgat and adrp for efficient replication. *Cell discovery* **7**, 1–13 (2021).

89. Swainston, N. *et al.* Recon 2.2: from reconstruction to model of human metabolism. *Metabolomics* **12**, 1–7, DOI: 10.1007/s11306-016-1051-4 (2016).

90. Python package index - pypi. https://pypi.org/.

91. Barrett, T. *et al.* NCBI GEO: archive for functional genomics data sets—update. *Nucleic acids research* **41**, D991–D995, DOI: 10.1093/nar/gks1193 (2012).

92. Huang, Y.-C. T. *et al.* Identification of gene biomarkers for respiratory syncytial virus infection in a bronchial epithelial cell line. *Genomic medicine* **2**, 113–125, DOI: 10.1007/s11568-009-9080-y (2008).

93. Norsigian, C. J. *et al.* BiGG Models 2020: multi-strain genome-scale models and expansion across the phylogenetic tree. *Nucleic Acids Res.* **48**, DOI: 10.1093/nar/gkz1054 (2019).

94. Geer, L. Y. *et al.* The NCBI BioSystems database. *Nucleic acids research* **38**, D492–D496, DOI: 10.1093/nar/gkp858 (2010).

95. Baltimore, D. Expression of animal virus genomes. *Bacteriol. reviews* **35**, 235–241, DOI: 10.1128/br.35.3.235-241.1971 (1971).

96. Keating, S. M. *et al.* SBML Level 3: an extensible format for the exchange and reuse of biological models. *Mol. Syst. Biol.* **16**, e9110, DOI: 10.15252/msb.20199110 (2020). https://www.embopress.org/doi/pdf/10.15252/msb.20199110.

97. Renz, A., Mostolizadeh, R. & Dräger, A. Clinical Applications of Metabolic Models in SBML Format. In Wolkenhauer, O. (ed.) *Systems Medicine*, vol. 3, 362–371, DOI: 10.1016/B978-0-12-801238-3.11524-7 (Academic Press, Oxford, 2020).

98. Malik-Sheriff, R. S. *et al.* BioModels—15 years of sharing computational models in life science. *Nucleic Acids Res.* **48**, D407–D415, DOI: 10.1093/nar/gkz1055 (2020).

99. Bergmann, F. T. *et al.* COMBINE archive and OMEX format: one file to share all information to reproduce a modeling project. *BMC Bioinforma.* **15**, 369, DOI: 10.1186/s12859-014-0369-z (2014).

100. Hastings, J. *et al.* ChEBI in 2016: Improved services and an expanding collection of metabolites. *Nucleic acids research* **44**, D1214–D1219, DOI: 10.1093/nar/gkv1031 (2016).

Preprints (www.preprints.org) | NOT PEER-REVIEWED | Posted: 27 July 2022 doi:10.20944/preprints202203.0290.v2

Supplementary Figures

Preprints (www.preprints.org) | NOT PEER-REVIEWED | Posted: 27 July 2022 doi:10.20944/preprints202203.0290.v2

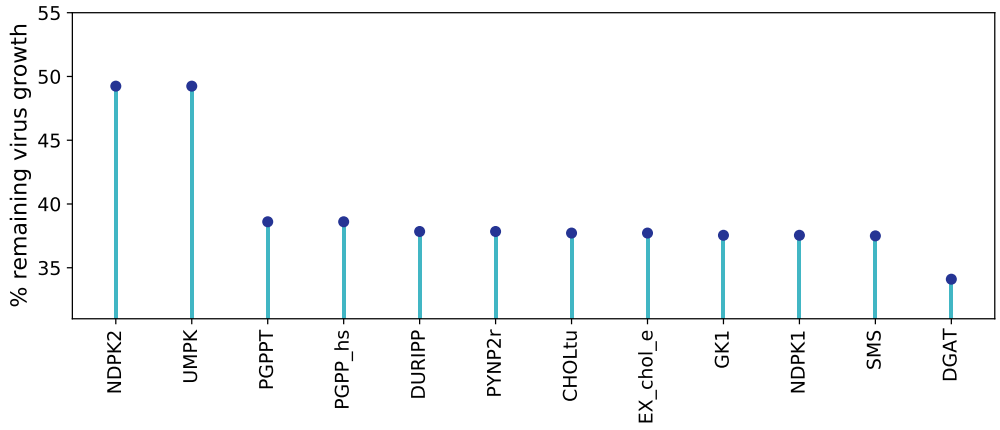

Figure A10. Results of the host-derived enforcement after defining the blood growth medium. After constraining the fluxes of NDPK1 and GK1, 37.5 % of the initial virus remained in the host. Compared to the minimal defined medium, diacylglycerol acyltransferase (DGAT) was proved to have a great impact on the virus growth leading to a decrease of 66 %.

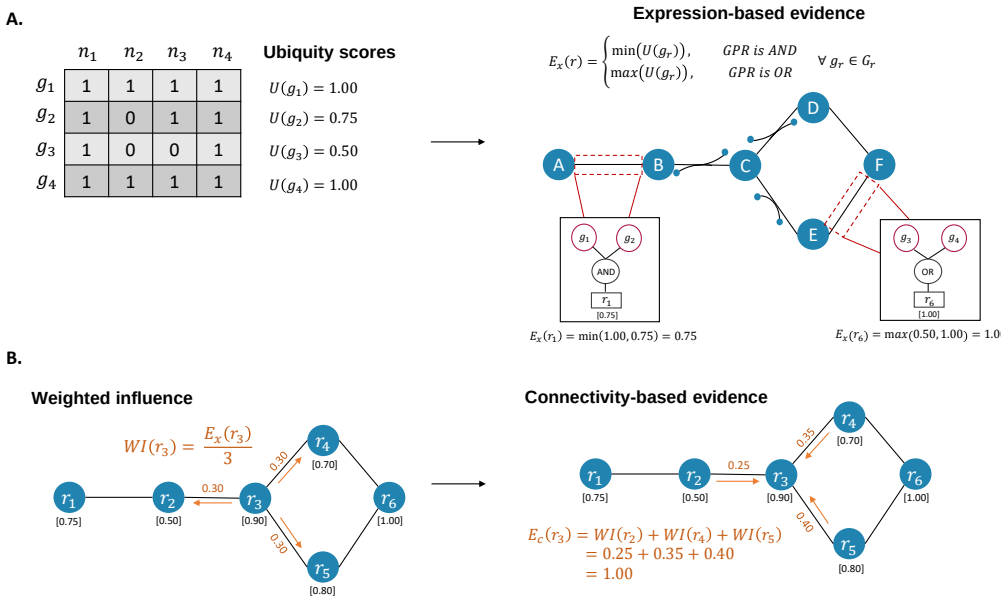

Figure A11. Overview of the evidence-based ranking of reactions in pymCADRE. The evidence-based ranking of reactions in pymCADRE is conducted similarly to mCADRE and consists of three main parts: (A) After binarizing tissue-specific data, the frequency of a gene's expression across all experiments of the same tissue is computed; this is the ubiquity score $U(g)$ for each gene g. The expression-based evidence $E_x(r)$ is computed for each gene-associated reaction r from ubiquity scores. Reactions with a sufficiently high $E_x(r)$ value are denoted as core reactions. Non-active reactions have zero expression-based evidence. (B) Non-core reactions are ranked based on the connectivity-based evidence $E_c(r)$, using the generic models' network topology and the weighted influence $WI(r)$. Figure re-created from Wang *et al.*[46].

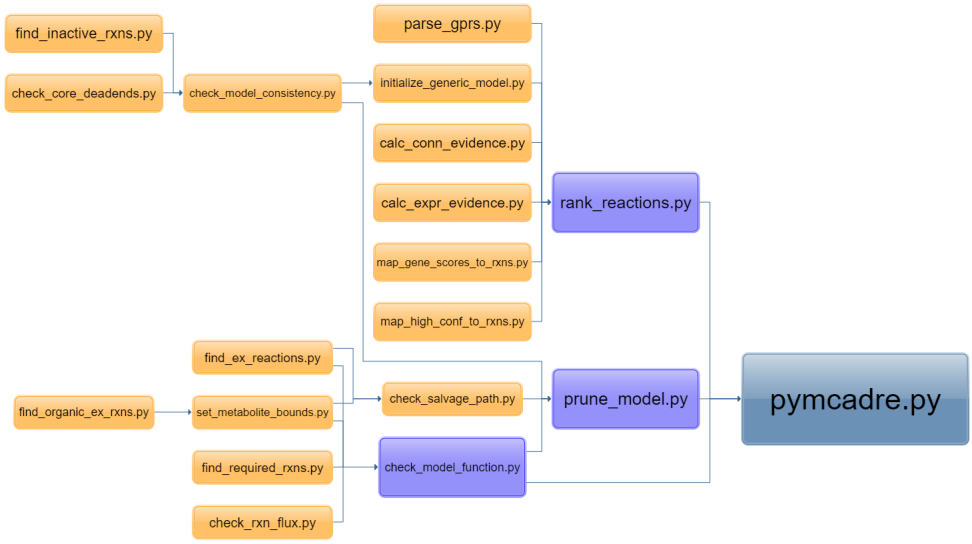

Figure A12. Hierarchical organization of the pymCADRE code and its dependencies. The three main scripts are colored with purple, while intermediate scripts are orange-colored. First of all, the `rank_reactions.py` module is executed, followed by `prune_model.py`. The module `check_model_function.py` is connected to main and intermediate scripts and is used multiple times within a single run.

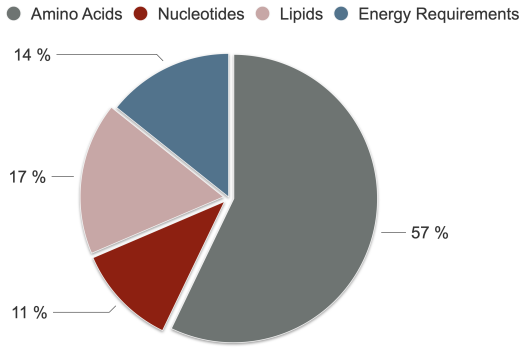

Figure A13. Categorization of the compounds needed for the growth of SARS-CoV-2. The VBOF includes totally four nucleotides, five energy-related metabolites, 20 proteinogenic amino acids, and six fatty acids.

Preprints (www.preprints.org) | NOT PEER-REVIEWED | Posted: 27 July 2022 doi:10.20944/preprints202203.0290.v2

1628 # Supplementary Tables

Table A4. Overview of compounds and their stoichiometric coefficients in the SARS-CoV-2 biomass function. From the listed metabolites, `adp_c`, `h_c`, `pi_c` and `ppi_c` are the products, while the rest the reactants.

Metabolite	Stoichiometric coefficient
adp_c	25.76630
atp_c	26.17860
ctp_c	0.25240
h_c	25.76630
h2o_c	25.76630
gly_c	0.49090
gtp_c	0.25240
pi_c	25.76630
ppi_c	0.66470
utp_c	0.41230
ala__L_c	0.51420
arg__L_c	0.36360
asn__L_c	0.35930
asp__L_c	0.27820
cys__L_c	0.10270
glu__L_c	0.20990
gln__L_c	0.30910
his__L_c	0.10110
ile__L_c	0.40210
leu__L_c	0.68620
lys__L_c	0.32490
met__L_c	0.10200
phe__L_c	0.29860
pro__L_c	0.28040
ser__L_c	0.49690
thr__L_c	0.44710
trp__L_c	0.12060
tyr__L_c	0.23500
val__L_c	0.31750
pchol_hs_c	0.03840
pe_hs_c	0.014566
pail_hs_c	0.006621
ps_hs_c	0.001986
chsterol_c	0.000012
sphmyln_hs_c	0.001986

Table A5. Amino acids and their three-letter and one-letter codes, and their molecular weight used to construct the SARS-CoV-2 VBOF. The molecular weights were derived from the ChEBI database[100]

Amino Acid	3-letter code	1-letter code	Molecular Weight
Alanine	Ala	A	89.1
Arginine	Arg	R	174.2
Asparagine	Asn	N	132.1
Aspartate	Asp	D	133.1
Cysteine	Cys	C	121.2
Glutamate	Glu	E	147.1
Glutamine	Gln	Q	146.2
Glycine	Gly	G	75.1
Histidine	His	H	155.2
Isoleucine	Ile	I	131.2
Leucine	Leu	L	131.2
Lysine	Lys	K	146.2
Methionine	Met	M	149.2
Phenylalanine	Phe	F	165.2
Proline	Pro	P	115.1
Serine	Ser	S	105.1
Threonine	Thr	T	119.1
Tryptophan	Trp	W	204.2
Tyrosine	Tyr	Y	181.2
Valine	Val	V	117.1

Table A6. Five-number summary of reaction fluxes in host and virus. The summary consists of five values: minimum, first quartile (25th percentile), median (50th percentile), third quartile (75th percentile), and maximum.

	host	virus
min	−3.71	−3.06
25 %	0.0	0.0
50 %	0.0	0.0
75 %	0.0	0.0
max	3.79	3.73